

**Rapid mass growth and enhanced light extinction of atmospheric aerosols during the heating season haze episodes in Beijing revealed by aerosol-chemistry-radiation-boundary layer interaction**

Zhuohui Lin<sup>1</sup>, Yonghong Wang<sup>2</sup>, Feixue Zheng<sup>1</sup>, Ying Zhou<sup>1</sup>, Yishuo Guo<sup>1</sup>, Zemin Feng<sup>1</sup>, Chang Li<sup>1</sup>, Yusheng Zhang<sup>1</sup>, Simo Hakala<sup>2</sup>, Tommy Chan<sup>2</sup>, Chao Yan<sup>2</sup>, Kaspar R. Daellenbach<sup>2</sup>, Biwu Chu<sup>3</sup>, Lubna Dada<sup>2</sup>, Juha Kangasluoma<sup>1,2</sup>, Lei Yao<sup>2</sup>, Xiaolong Fan<sup>1</sup>, Wei Du<sup>2</sup>, Jing Cai<sup>2</sup>, Runlong Cai<sup>2</sup>, Tom V. Kokkonen<sup>2,4</sup>, Putian Zhou<sup>2</sup>, Lili Wang<sup>5</sup>, Tuukka Petäjä<sup>2,4</sup>, Federico Bianchi<sup>1,2</sup>, Veli-Matti Kerminen<sup>2,4</sup>, Yongchun Liu<sup>1</sup>, and Markku Kulmala<sup>1,2,4</sup>

<sup>1</sup>Aerosol and Haze Laboratory, Beijing Advanced Innovation Center for Soft Matter Science and Engineering, Beijing University of Chemical Technology, Beijing, China

<sup>2</sup>Institute for Atmospheric and Earth System Research / Physics, Faculty of Science, University of Helsinki, Finland

<sup>3</sup>Research Center for Eco-Environmental Sciences, Chinese Academy of Science, Beijing, China

<sup>4</sup>Joint international research Laboratory of Atmospheric and Earth System sciences (JirLATEST), Nanjing University, Nanjing, China

<sup>5</sup>State Key Laboratory of Atmospheric Boundary Layer Physics and Atmospheric Chemistry (LAPC), Institute of Atmospheric Physics, Chinese Academy of Sciences, Beijing 100029, China

Corresponding author: Yonghong Wang

E-mail: yonghong.wang@helsinki.fi

Revised to: Atmospheric Chemistry and Physics

27   **Abstract**

28

29   Despite the numerous studies investigating haze formation mechanism in China, it is still puzzling  
30   that intensive haze episodes could form within hours directly following relatively clean periods. Haze  
31   has been suggested to be initiated by the variation of meteorological parameters and then to be  
32   substantially enhanced by aerosol-radiation-boundary layer feedback. However, knowledge on the  
33   detailed chemical processes and the driving factors for extensive aerosol mass accumulation during  
34   the feedback is still scarce. Here, the dependency of the aerosol number size distribution, mass  
35   concentration and chemical composition on the daytime mixing layer height (MLH) in urban Beijing  
36   is investigated. The size distribution and chemical composition-resolved dry aerosol light extinction  
37   is also explored. The results indicate that the aerosol mass concentration and fraction of nitrate  
38   increased dramatically when the MLH decreased from high to low conditions, corresponding to  
39   relatively clean and polluted conditions, respectively. Particles having their dry diameters in the size  
40   of ~400-700 nm, and especially particle-phase ammonium nitrate and liquid water, contributed  
41   greatly to visibility degradation during the winter haze periods. The dependency of aerosol  
42   composition on the MLH revealed that ammonium nitrate and aerosol water content increased the  
43   most during low MLH conditions, which may have further triggered enhanced formation of sulphate  
44   and organic aerosol via heterogeneous reactions. As a result, more sulphate, nitrate and water soluble  
45   organics were formed, leading to an enhanced water uptake ability and increased light extinction by  
46   the aerosols. The results of this study contribute towards a more detailed understanding of the aerosol-  
47   chemistry-radiation-boundary layer feedback that is likely to be responsible for explosive aerosol  
48   mass growth events in urban Beijing.

49

50

51

52

53

54

## 55 1. Introduction

56 Despite the recent reduction of air pollutants and their precursors in China between 2013 and 2017,  
57 the current emission and air pollution levels are still substantially high (Wang et al., 2020b; Zheng et  
58 al., 2018). Such high emissions, combined with specific meteorological conditions, frequently lead  
59 to severe haze episodes (An et al., 2019; Wang et al., 2019). Particulate matter, a major air pollutant,  
60 has considerable effects on climate, human health and visibility degradation (Che et al., 2007;  
61 Lelieveld et al., 2015; Spracklen et al., 2008; Wang et al., 2015).

62  
63 During winter haze episodes, a rapid growth of the aerosol mass concentration has commonly been  
64 observed, and this phenomenon seems to be directly affected by meteorological factors (Li et al.,  
65 2018b; Liu et al., 2018, 2019b; Wang et al., 2018a, 2014a). The meteorological conditions and  
66 increased aerosol concentrations are proposed to be interlinked by a feedback loop, called the aerosol-  
67 chemistry-boundary layer feedback, in which aerosol particles reduce both solar radiation reaching  
68 the surface and turbulent kinetic energy of the near-surface air (Ding et al., 2016; Petäjä et al., 2016;  
69 Wang et al., 2020d). The increased stability of the boundary layer leads to enhanced air pollution in  
70 the mixed layer, which further suppresses the development of boundary layer. As a consequence,  
71 concentrations of primary aerosol particles, water vapor and relative humidity increase, creating more  
72 favourable conditions for homogeneous and heterogeneous on aerosol surfaces or inside them (Cheng  
73 et al., 2016a; Wang et al., 2016; Wu et al., 2018). Such reactions cause rapid formation of secondary  
74 aerosol matter and enhanced light extinction during severe winter haze episodes. However, more  
75 detailed information on the aerosol and reactive gas chemistry during the aerosol-chemistry-boundary  
76 layer feedback and related rapid aerosol mass growth events is still needed (Liu et al., 2019). For  
77 instance, it is still unclear which chemical reactions and which compounds in the particulate matter  
78 play key roles during such rapid mass growth events.

79  
80 The particle number size distribution and chemical composition are considered to be the most  
81 important variables influencing the light extinction by aerosol particles. In the atmosphere, the highest  
82 contribution to aerosol light extinction comes from organic compounds, nitrate and sulphate in

particles with diameters of 100-1000 nm. This is due to the dominant mass fractions of the aforementioned compounds in aerosols that correspond to the peak intensity of solar radiation at wavelengths around 550 nm (Jimenez et al., 2009; Swietlicki et al., 2008). In addition, light scattering which contributes the most to the light extinction by atmospheric aerosols, can be substantially enhanced by the presence of liquid water in the aerosol (Chen et al., 2014; Liu et al., 2019a; Pan et al., 2009; Wang et al., 2020). Hence, quantifying the response of light extinction to different chemical compounds would be helpful in evaluating the feedbacks associated with secondary aerosol production.

In this study, we focus on the physical and chemical properties of aerosols in Beijing during the winter heating season from October 2018 to February 2019 using state-of-the-art instrumentation. The variation of aerosol chemical composition and the associated light extinction coefficient as a function of the varying mixing layer height are discussed. Our aim is to identify the key chemical components which contribute to the aerosol-chemistry-radiation-boundary layer feedback loop in Beijing.

## 2. Methodology

### 2.1. Measurement location and instrumentations

Measurements were conducted between 1 October 2018 and 28 February 2019 at the roof top of the university building at the west campus of Beijing University of Chemical Technology (39.95°N, 116.31°E). This station is located about 150 m away from the nearest road (Zizhuyuan road) and 500 m away from the West Third Ring Road, and it is surrounded by commercial properties and residential dwellings representative of an urban environment. More details on the location can be found in (Liu et al., 2020; Zhou et al., 2020).

The meteorological data for this work include basic meteorological variables (relative humidity (RH), temperature, wind speed, wind direction, and visibility) and mixing layer height (MLH) measured

109 using a weather station (Vaisala Inc., Finland) and a Ceilometer CL51 (Vaisala Inc., Finland),  
110 respectively. The MLH is defined as the height above the surface, through which relatively vigorous  
111 vertical mixing occurs (Holzworth, 1972), and its value is highly related to the vertical temperature  
112 structure and, to some extent, to a mechanically-induced turbulence (Baxter, 1991). Here, we  
113 followed the method introduced earlier by Mönkel et al. (2007) and Eresmaa et al. (2012) in  
114 determining the MLH.

115

116 The number concentration of clusters or small aerosol particles in the size range from 1.3-2.5 nm and  
117 the number size distributions of aerosol particles from 6 nm to 840 nm were measured by a Particle  
118 Sizer Magnifier (PSM) and a Differential Mobility Particle Sizer (DMPS), respectively (Aalto et al.,  
119 2001; Vanhanen et al., 2011). The mass concentration of fine particulate matter (PM<sub>2.5</sub>) was measured  
120 using a Tapered Element Oscillating Microbalance Dichotomous Ambient Particulate Monitor  
121 (TEOM 1405-DF, Thermo Fisher Scientific Inc, USA) with a total flow rate of 16.67 L/min (Wang  
122 et al., 2014).

123

124 A time-of-flight aerosol chemical speciation monitor (ToF-ACSM, Aerodyne Research Inc.) was used  
125 to measure the concentrations of non-refractory (NR) components, including sulfate, nitrate,  
126 ammonium, chloride and organics of PM<sub>2.5</sub> (Fröhlich et al., 2013). [A PM<sub>2.5</sub> cyclone was deployed on  
the rooftop with a flow rate of 3 L /min. Aerosol was dried through a Nafion dryer \(MD-700-24F-3,  
PERMA PURE\) before entering the ToF- ACSM.](#) The inlet flow was set at 1.4 cm<sup>3</sup>/s. The particle  
129 beam passed through the chamber and reached the heated porous tungsten surface (T≈600°C). There,  
130 the non-refractory PM<sub>2.5</sub> constituents were vaporized and then ionized by electrons (E<sub>kin</sub>=70eV,  
131 emitted by a tungsten filament). The ions were measured by a detector and the data was analyzed  
132 using Tofware ver. 2.5.13 within IgorPro ver. 6.3.7.2 (WaveMetrics). The relative ionization  
133 efficiencies (RIE) for sulfate, nitrate, ammonium, chloride and organics applied were 0.86, 1.05, 4.0,  
134 1.5 and 1.4, respectively. [Except RIE correction, the data also did CO<sub>2</sub>+ / NO<sub>3</sub> artifact correction  
\(Pieber et al., 2016\) and collection efficiency \(CE\) correction \(Middlebrook et al., 2012\).](#) Mass  
136 concentrations of ammonium nitrate, ammonium sulfate and ammonium chloride were determined

137 according to the method introduced by Gysel et al. (2007). The aerosol liquid water content (AWC)  
138 was calculated by thermodynamic equilibrium model ISORROPIA II using ToF-ACSM data  
139 (Fountoukis and Nenes, 2007).

140 Highly-oxygenated organic molecules (HOMs) were measured by a chemical ionization long time-  
141 of-flight mass spectrometer equipped with a nitrate chemical ionization source (LToF-CIMS,  
142 Aerodyne Research, Inc. USA) (Jokinen et al., 2012) similar to gas-phase sulfuric acid. The ambient  
143 air was drawn into the ionization source through a stainless-steel tube with a length of ~1.6 m and a  
144 diameter of 3/4 inch at a flowrate of ~ 8 L/min. A 30-40 L/min purified air flow and a 4-8 mL/min  
145 ultrahigh purity nitrogen flow containing nitric acid were mixed together as the sheath flow, which is  
146 guided through a PhotoIonizer (Model L9491, Hamamatsu, Japan) to produce nitrate reagent ions.  
147 This sheath flow is then introduced into a co-axial laminar flow reactor concentric to the sample flow.  
148 Nitrate ions are pushed to the sample flow layer by an electric field and subsequently charge analytical  
149 molecules. Organic carbon (OC) and element carbon (EC) concentrations were measured semi-  
150 continuously with a 1-hour time resolution using an OC/EC Analyzer (Model-4, Sunset Lab. Inc.).  
151 The ammonia is measured by Trace Ammonia analyzer ( Los Gatos Research, Inc.) at atmospheric  
152 ambient levels with high precision (0.2 ppb in 1s) and ultra-fast response (5 Hz).

153

154 The air mass history was studied by calculating particle retroplumes using a Lagrangian particle  
155 dispersion model FLEXPART (FLEXible PARTicle dispersion model) ver. 9.02 (Stohl et al., 2005).  
156 The ECMWF (European Centre for Medium-Range Weather Forecast) operational forecast (with 0.15°  
157 horizontal and 1 h temporal resolution) was used as the meteorological input into the model. During  
158 the measurement period, a new release of 50 000 test particles, distributed evenly between 0 and 100  
159 m above the measurement site, occurred every 1 hour. The released particles were traced backwards  
160 in time for 72 h, unless they exceeded the model boundary (20–60°N, 95–135°E).

161

## 162 **2.2. Aerosol light extinction calculation**

163 The aerosol light extinction coefficient was calculated with the Mie-Model, which uses particle

number size distribution, mass concentrations of different aerosol compounds and their refractive index as inputs (Seinfeld and Pandis, 2006). We introduced a series of assumptions into the Mie-Model, including 1) “internal mixture” which considers each chemical component in a particle as homogeneously mixed with each other; 2) all particles are spherical; and 3) particles of different sizes have the same chemical composition.

The practical method introduced under those assumptions in previous studies were found to be capable of estimating a variation trend of optical property of PM<sub>0.5–20</sub> with a relatively good accuracy (Lin et al., 2013).

Table 1. Summary of the parameters for calculating the average optical refractive index.

Species	$\rho_i (\text{g cm}^{-3})$	$n_i$	$k_i$
(NH <sub>4</sub> ) <sub>2</sub> SO <sub>4</sub>	1.760	1.530	0.000
NH <sub>4</sub> NO <sub>3</sub>	1.725	1.554	0.000
NH <sub>4</sub> Cl	1.527	1.639	0.000
Organics	1.400	1.550	0.001
EC	1.500	1.800	0.540

The average optical refractive index (AORI) of an internally-mixed particle can be calculated from the optical refractive indices (ORI) of each chemical component by following a mixing rule of volume-averaged chemical components as  $\text{AORI} = n_{\text{eff}} + k_{\text{eff}} \times i$ , where the real part ( $n_{\text{eff}}$ ) and imaginary part ( $k_{\text{eff}}$ ) are given by:

$$n_{\text{eff}} = \left( \sum_i n_i \cdot m_i / \rho_i \right) / \left( \sum_i m_i / \rho_i \right) \quad (1)$$

$$k_{\text{eff}} = \left( \sum_i k_i \cdot m_i / \rho_i \right) / \left( \sum_i m_i / \rho_i \right) \quad (2)$$

Here  $m_i$  and  $\rho_i$  are the mass concentration and density of the component  $i$  in particles, respectively,

182 and  $n_i$  and  $k_i$  are the real and imaginary parts of ORI of this component, respectively. The  
 183 parameters for calculating the AORI are summarised in Table 1. The values of  $n_i$  and  $k_i$  in Table 1  
 184 are referenced to the light wavelength of 550 nm.

185  
 186  $Q_{sp,j}$  represents light scattering efficiency of a single particle with diameter  $D_j$ , while  $Q_{ep,j}$   
 187 represents light absorption efficiency. Theoretically,  $Q_{sp,j}$  and  $Q_{ep,j}$  are both the function of  $D_j$  and  
 188 the  $AORI_j$  (the AORI of the particle with diameter  $D_j$ ) at a given light wavelength  $\lambda$ , for which the  
 189 complicated calculations were referenced to a previous publication (Lin et al., 2013). Regarding the  
 190 limitations of measurement techniques, the  $AORI_j$  was assumed to be equal to the  $AORI_{PM2.5}$ , which  
 191 was determined based on chemical composition of  $PM_{2.5}$ . It is possible to derive expressions for the  
 192 cross sections of a spherical particle exactly. The formulas for  $Q_{sp,j}$  and  $Q_{ep,j}$  are:

193

$$Q_{sp,j}(D_j, \lambda, AORI_j) = \frac{2}{\alpha^2} \sum_{k=1}^{\infty} (2k+1) \cdot [|a_k|^2 + |b_k|^2] \quad (3)$$

$$Q_{ep,j}(D_j, \lambda, AORI_j) = \frac{2}{\alpha^2} \sum_{k=1}^{\infty} (2k+1) \cdot \text{Re}[a_k + b_k] \quad (4)$$

194

195 where

196

$$197 \quad a_k = \frac{\alpha \psi'_k(y) \psi_k(\alpha) - y \psi'_k(\alpha) \psi_k(y)}{\alpha \psi'_k(y) \xi_k(\alpha) - y \xi'_k(\alpha) \psi_k(y)}$$

198

$$199 \quad b_k = \frac{y \psi'_k(y) \psi_k(\alpha) - \alpha \psi'_k(\alpha) \psi_k(y)}{y \psi'_k(y) \xi_k(\alpha) - \alpha \xi'_k(\alpha) \psi_k(y)}$$

200

201 with  $y = \alpha m$ .

202

$$203 \quad m = n_{eff} + i \cdot k_{eff}$$

204



$$\alpha = \frac{\pi D_j}{\lambda}$$

with  $\lambda = 550$  nm.

where complex number  $m$  stands for  $AORI_j$ , while  $\alpha$  is the size of the particle, usually expressed as a dimensionless size parameter. The functions  $\psi_k(z)$  and  $\xi_k(z)$  are the Riccati–Bessel functions:

$$\psi_k(z) = \left(\frac{\pi z}{2}\right)^{1/2} J_{k+1/2}(z) \quad (5)$$

$$\xi_k(z) = \left(\frac{\pi z}{2}\right)^{1/2} [J_{k+1/2}(z) + i(-1)^k J_{-k-1/2}(z)] \quad (6)$$

where  $J_{k+1/2}$  and  $J_{-k-1/2}$  are the Bessel functions of the first kind and their footnotes indicate the order of Bessel functions. The Mie theory can serve as the basis of a computational procedure to calculate the scattering and absorption of light by any sphere as a function of wavelength.

According to the Mie-Model,  $b_{sp}$  (light scattering coefficient) and  $b_{ep}$  (light extinction coefficient) can be quantified with Eqs. (5) and (6), respectively.  $b_{ap}$  (light absorption coefficient) is the difference between  $b_{ep}$  and  $b_{sp}$ , which equals zero, when  $k_i$  equals zero or very small. Optical properties including  $b_{ep}$ ,  $b_{sp}$  and  $b_{ap}$  to be discussed later are all referenced to light wavelength of 550 nm.

$$b_{sp} = \sum_j b_{sp,j} = \sum_j \frac{\pi D_j^2}{4} \cdot Q_{sp,j}(D_j, \lambda, AORI_j) \cdot N_j \quad (7)$$

$$b_{ep} = \sum_j b_{ep,j} = \sum_j \frac{\pi D_j^2}{4} \cdot Q_{ep,j}(D_j, \lambda, AORI_j) \cdot N_j \quad (8)$$

In Eqs. (7) and (8),  $D_j$  stands for the median Stokes diameter in the  $j$ -th particle size range and  $N_j$  is the number concentration of particles with diameter,  $D_j$ .

### 226 3. Results and discussion

#### 227 3.1. Typical case of rapid aerosol mass growth episodes affected by aerosol-chemistry- 228 boundary layer interactions

229 An example of rapid aerosol mass growth in urban wintertime Beijing is illustrated in Figure 1, where  
230 the haze accumulation was associated with a rapid PM<sub>2.5</sub> mass concentration increase from 8.5 µg/m<sup>3</sup>  
231 to more than 100 µg/m<sup>3</sup> in less than 7 hours. A haze episode started on afternoon 20 February 2019  
232 under stagnant meteorological conditions with low wind speeds and elevated ambient relative  
233 humidity (Figure S1). The polluted periods during this case occurred under southerly wind transport  
234 conditions, whereas clean air masses originated from the north-westerly regions (as shown in Figure  
235 S2, S3). These are typical features for a haze evolution process in Beijing (Wang et al., 2020b). During  
236 the haze periods marked by the shaded areas in Figure 1, an obvious increase of chemical mass  
237 concentration was observed by the ToF-ACSM, characterised by high concentrations of secondary  
238 aerosol components (nitrate, organics and sulphate) and typically a shallow boundary layer. The mass  
239 concentrations of organics, sulphate and nitrate increased dramatically with a decreasing MLH,  
240 accounting for 88.5% of NR-PM<sub>2.5</sub> (non-refractory PM<sub>2.5</sub>) during the rapid aerosol mass growth  
241 period. The aerosol mass growth was the fastest for nitrate. The mass concentrations of organic and  
242 elemental carbon followed that of NR-PM<sub>2.5</sub>.

243  
244 The MLH reached its maximum at around 14:00 in the afternoon of 20 February, after which the  
245 development of the mixing layer was suppressed and MLH decreased with the arrival of pollution  
246 (Figure 1a). Previous studies have shown that the aerosol-radiation-boundary layer feedback  
247 contributes to a rapid enhancement of air pollution (Petäjä et al., 2016; Wang et al., 2020d). High  
248 concentrations of aerosol particles obscure downward radiation, as a result of which the surface  
249 temperature and sensitive heat flux decrease and the development of mixing layer height is suppressed.  
250 Recent studies have gradually realized that the facilitation of various chemical processes play a non-  
251 negligible role in the aerosol-radiation-boundary layer feedback (Liu.Q et al., 2018; Liu. Z et al., 2019).  
252 Therefore, it is important to identify and quantify the role of different specific chemical species and

particle size ranges in reducing atmospheric radiation and extinction.

Figure 2 shows the contributions of size and chemical composition-resolved dry aerosol to light extinction during the investigated period. As the pollution intensified and MLH decreased (Fig 1c), the light extinction of atmospheric aerosols increased significantly. Assuming that particles of different sizes have the same chemical composition as  $\text{PM}_{2.5}$  (organics,  $\text{NH}_4\text{NO}_3$ , EC,  $(\text{NH}_4)_2\text{SO}_4$ ,  $\text{NH}_4\text{Cl}$ ), the light extinction of particles in the size range of 300-700 nm increased significantly from the relative clean period to the polluted period (namely from 12:00 to 16:00). During relatively clean conditions, the contributions of organics,  $\text{NH}_4\text{NO}_3$ , EC,  $(\text{NH}_4)_2\text{SO}_4$  and  $\text{NH}_4\text{Cl}$  to the total aerosol light extinction were 42%, 23%, 18%, 11% and 7%, respectively. The contribution of  $\text{NH}_4\text{NO}_3$  to aerosol light extinction reached 40% during the heavily polluted period. Based on the observation it is likely that the increased light extinction by aerosols reduced solar radiation reaching the surface, so that the development of the boundary layer was suppressed.

### 3.2. Connection between the aerosol chemical composition, light extinction, size distribution and MLH during the heating season

To better characterize the effect of the chemical composition of dry aerosols and the PNSD (particle number size distribution) light extinction under different MLH conditions, the daytime (8:00 – 16:00 LT) measurement data from October 2018 to February 2019 were selected for further analysis. As shown by Figure 3 and consistent with other observations in Beijing (Tang et al., 2016; Wang et al., 2020c), there was a general tendency for the  $\text{PM}_{2.5}$  mass concentration to increase with a decreasing MLH. Organic compounds and nitrate were the most abundant fractions of the daytime aerosol mass composition, contributing together approximately 70% to total  $\text{NR-PM}_{2.5}$  mass concentration. With a decreasing MLH, the fraction of nitrate mass in  $\text{NR-PM}_{2.5}$  slightly increased while that of organics decreased. This feature makes the aerosol more hygroscopic under low MLH conditions typical for heavily polluted periods. The increased nitrate fraction in the aerosol could also enhance the

280 formation of other secondary aerosol components (Xue et al., 2019). Note that some fraction of  
281 aerosol nitrate could consist of organic nitrate originating from reaction of peroxy radical with nitric  
282 oxide; however, it is difficult to distinguish organic nitrate from inorganic nitrate at the moment due  
283 to instrumental limitations (Fröhlich et al., 2013).

284

285 Figure 4 depicts the calculated daytime light extinction of the dry aerosol as a function of the MLH,  
286 separated by different size ranges and chemical components. We may see that in general, particles  
287 with dry diameters in the range of 300-700 nm explains more than 80% of the total aerosol light  
288 extinction (Figure 4b). Similar to their share in NR-PM<sub>2.5</sub>, the fraction of light extinction by  
289 ammonium nitrate increased and that of organics decreased during the lowest MLH conditions  
290 corresponding to the heavy pollution periods (Figure 4d). There are also apparent differences in the  
291 relative contribution of different particle size ranges to light extinction in different MLH conditions:  
292 with a decreasing MLH, the contribution of particles with dry dimeters larger than about 400-500 nm  
293 clearly increased while that of sub-300 nm particles notably decreased. This indicates that the  
294 enhanced light extinction by the dry aerosol at low MLH conditions was not only due the more  
295 abundant aerosol mass concentration, but also due to the growth of individual particles to optically  
296 more active sizes.

297

298 At relative humidity larger than about 70%, aerosol liquid water gives a significant contribution to  
299 the aerosol mass concentration and often a dominant contribution to the aerosol light extinction (Titos  
300 et al., 2016). This has important implications for the aerosol-chemistry-radiation-boundary layer  
301 feedback, when considering our findings listed above and further noting that heavy pollution periods  
302 are often accompanied by high values of RH in Beijing (Zhong et al., 2018). First, compared to clean  
303 or moderately-polluted conditions, the enhancement in the aerosol light extinction under polluted is  
304 probably much larger than that illustrated in Figure 4. Second, the high aerosol water content under  
305 polluted conditions promotes many kinds of chemical reactions taking place on the surface or inside  
306 aerosol particles.

307

### 3.3. Aerosol-chemistry-radiation-boundary layer interaction

In order to further investigate the interaction between MLH and chemical compounds (either observed or calculated), we divided the observed PM<sub>2.5</sub> concentrations into highly polluted and less polluted conditions using a threshold value of 75  $\mu\text{g}/\text{m}^3$  for PM<sub>2.5</sub>. The organics, nitrate, ammonium, sulfate, chloride, HOM, aerosol water content (AWC) and PM<sub>2.5</sub> as a function of the mixing layer height during both highly polluted and less polluted conditions are shown in Figure 5. The fitted relationships connecting the concentrations of different chemical compounds to the reduction of MLH under highly and less polluted conditions allowed us to estimate the net mass concentration increase of each compound due to secondary formation and aerosol-chemical-boundary layer feedback under highly polluted conditions (shaded areas in Figure 5). It is worth noting that AWC, nitrate and sulfate increased the most as the MLH decreased, as represented by the large shaded areas in Figs. 5 (h), (b) and (c). The day-time nitrate in aerosol is formed predominately via the reaction of nitric acid and ammonium, while nitric acid is produced from gas phase reaction of nitrogen dioxide and hydroxy radical (Seinfeld and Pandis, 2006). High concentrations of daytime nitrate aerosols indicate efficient production of gas phase nitric acid, its partitioning into liquid aerosol and its fast neutralization by abundant ammonia (Li et al., 2018a; Pan et al., 2016; Wang et al., 2020). A recent study shows that condensation of nitric acid and ammonia could promote fast growth of newly formed particle in urban environment condition (Wang et al., 2020d). Another possibility is that ammonium nitrate is formed rapidly on particle surfaces due to the hydrolysis of dinitrogen pentoxide (N<sub>2</sub>O<sub>5</sub>) during daytime, as the AWC increased significantly (Wang et al., 2014; Wang et al., 2020). However, a quantitative distinction between the two formation pathways for nitrate formation is not possible in this study. The dramatic increase of nitrate aerosol could also promote the formation of sulfate by heterogeneous reactions (Cheng et al., 2016b; Wang et al., 2016). The concentration of HOMs showed a slight increase as the MLH decreased, which suggests that also the formation of HOMs is enhanced with an increased level of air pollution. This phenomenon should be further investigated as HOMs can substantially contribute to the secondary organic aerosol formation.

336 Figure 6 displays the dry aerosol light extinction by different chemical compounds in the same way  
337 as Fig. 5 did for aerosol mass concentrations. The aerosol light extinction is directly related to the  
338 reduction of solar radiation reaching the surface, assuming that aerosol chemical components are  
339 vertically nearly homogeneously distributed. The light extinction from ammonium nitrate,  
340 ammonium sulfate and organics showed significantly increased contributions under highly polluted  
341 conditions (low MLH) as compared with less polluted conditions. To the contrary, no such  
342 enhancement was observed for ammonium chloride or element carbon (Figs. 6 (d) and (e)). In case  
343 of EC this is an expected result, as it originates solely from primary sources. The formation of particle  
344 phase chloride have secondary sources from chlorine atom-initiated oxidation of volatile organic  
345 compounds, so that the resulting oxidation products could contribute to the observed chloride (Wang  
346 and Ruiz, 2017; Wang et al., 2019a).

347

348 To better illustrate the combined effects of secondary aerosol formation and associated feedback on  
349 the daytime mass concentrations and light extinction due to different chemical components, we scaled  
350 these quantities by either the total PM<sub>2.5</sub> mass concentration or EC concentration and plotted them as  
351 a function of MLH (Fig. 7). The latter scaling minimizes the boundary layer accumulation effect on  
352 our analysis, as EC originates from primary emission sources (Cao et al., 2006). As shown in Fig. 7a,  
353 organics with their mass fraction of 61% were the most abundant component in PM<sub>2.5</sub> under high  
354 MLH conditions, followed by nitrate and ammonium with their mass fractions of 22% and 13%,  
355 respectively. The aerosol was estimated to be rather dry under high MLH conditions ( $AWC/PM_{2.5} =$   
356 0.03). However, with the decreasing MLH, the fraction of nitrate and the AWC to PM<sub>2.5</sub> ratio increased  
357 up to 45% and 0.2, respectively. This clearly indicates rapid nitrate formation and dramatic increase  
358 of the aerosol water uptake from less polluted conditions to intensive haze pollution. Compared with  
359 EC (Fig.7c), the concentrations of organic compounds, nitrate, sulfate and ammonium increased by  
360 factors of 1.5, 6.3, 4.8 and 4.9 respectively, from the highest to the lowest MLH conditions. Thus,  
361 although organics remained as the second most abundant aerosol component after nitrate under haze  
362 conditions, secondary formation and associated feedback from less to highly polluted conditions were  
363 clearly stronger for both sulfate and ammonium. Efficient sulfate production associated with haze

364 formation has been reported in several studies conducted in China (Cheng et al., 2016; Xie et al.,  
365 2015; Xue et al., 2016). Ammonium production during haze formation is tied with neutralization of  
366 acidic aerosol by ammonia, which was apparently present abundantly in the gas phase. Compared  
367 with the EC concentration, light extinction by ( $\text{NH}_4\text{NO}_3$ ) increased the most from the highest MLH  
368 conditions ( $248 \text{ M m}^{-1}/\mu\text{g m}^{-3}$ ) to the lowest MLH conditions ( $1150 \text{ M m}^{-1}/\mu\text{g m}^{-3}$ ) as shown by Figure  
369 7b. Overall, the rapid growth of nitrate aerosol mass, together with abundant concentration of organic  
370 aerosol, were the main cause of the light extinction for dry aerosol under haze formation.

371

372 The mechanism governing the aerosol-chemistry-radiation-boundary layer feedback for the rapid  
373 growth of atmospheric aerosol is illustrated in Fig. 8. As a result of reduction in solar radiation and  
374 atmospheric heating, a variety of chemical reactions in the gas phase and on particle surfaces or inside  
375 them are enhanced with an increased relative humidity and AWC. Such conditions are unfavorable  
376 for the dispersion of pollutants, which further enhances atmospheric stability. The formation of  
377 hydrophilic compounds, e.g., nitrate, sulfate and oxygenated organic compounds, result in enhanced  
378 water uptake by aerosol particles, which will essentially increase heterogeneous reactions associated  
379 with these particles. As a result, the aerosol mass and size increase, light extinction is enhanced, and  
380 the development of the mixing layer is depressed. At the same time, aerosol precursors concentrated  
381 within a shallower mixing layer lead to enhanced production rate of aerosol components in both gas  
382 and aerosol phases, especially nitrate but also other secondary aerosol. The increased concentrations  
383 of aerosol will further enhance this positive loop.

384

#### 385 4. Conclusions

386

387 We investigated the synergetic variations of aerosol chemical composition and mixing layer height  
388 during the daytime in urban Beijing. Significant dependency of the sharp increase of ammonium  
389 nitrate and aerosol water content with the occurrence of the explosive aerosol mass growth events  
390 were observed. We showed that these two components drove a positive aerosol-chemistry-radiation-

boundary layer feedback loop, which played an important role in the explosive aerosol mass growth events. A plausible explanation is that the increased aerosol water content at low mixing layer heights provides favorable conditions for heterogeneous reactions for nitrate and sulfate production and neutralization by ammonia. The significant formation of secondary aerosol increases the concentration of aerosol particles in the diameter range 300-700 nm, which effectively reduces the solar radiation reaching the surface and further enhances the aerosol-chemistry-radiation-boundary layer feedback loop. Our analysis connects the aerosol light extinction to a reduction in the mixing layer height, which suppresses the volume into which air pollutants are emitted and leads to an explosive aerosol mass growth. Our results indicate that reduction of ammonium and nitrate concentration in aerosol could weaken the aerosol-radiation-chemistry-boundary layer feedback loop, which could thereby reduce heavy haze episodes in Beijing.

## **5. Acknowledgements**

This work was supported by the funding from Beijing University of Chemical Technology. The European Research Council via advanced grant ATM-GTP (project no. 742206) and Academy of Finland via Academy professor project of M. K.

## **6. Competing financial interests**

The authors declare no competing financial interests.

## **7. Author contributions**

YW and MK initiated the study. ZL, YW, FZ, YZ, YG, ZF, CL, YZ, TC, CY, KD, BC, JK, LY, XF, WD, JC and YL conducted the longtime measurements. ZL, YW, LD, RC, SH, PZ, LW, VK, YL and MK interpreted the data. ZL, YW and VK wrote the manuscript.





- Aalto, P., Hämeri, K., Becker, E. D. O., Weber, R., Salm, J., Mäkelä, J. M., Hoell, C., O'Dowd, C. D., Karlsson, H., Hansson, H., Väkevä, M., Koponen, I. K., Buzorius, G. and Kulmala, M.: Physical characterization of aerosol particles during nucleation events, *Tellus, Series B: Chemical and Physical Meteorology*, 53(4), 344–358, doi:10.3402/tellusb.v53i4.17127, 2001.
- An, Z., Huang, R.-J., Zhang, R., Tie, X., Li, G., Cao, J., Zhou, W., Shi, Z., Han, Y., Gu, Z. and Ji, Y.: Severe haze in northern China: A synergy of anthropogenic emissions and atmospheric processes, *Proceedings of the National Academy of Sciences*, 116(18), 8657 LP – 8666, doi:10.1073/pnas.1900125116, 2019.
- Baxter, R.: Determination of mixing heights from data collected during the 1985 SCCCAMP field program, *Journal of Applied Meteorology*, 30(5), 598–606, doi:10.1175/1520-0450(1991)030<0598:DOMHFD>2.0.CO;2, 1991.
- Cao, G., Zhang, X. and Zheng, F.: Inventory of black carbon and organic carbon emissions from China, *Atmospheric Environment*, 40(34), 6516–6527, doi:10.1016/j.atmosenv.2006.05.070, 2006.
- Che, H., Zhang, X., Li, Y., Zhou, Z. and Qu, J. J.: Horizontal visibility trends in China 1981-2005, *Geophysical Research Letters*, 34(24), doi:10.1029/2007GL031450, 2007.
- Chen, J., Zhao, C. S., Ma, N. and Yan, P.: Aerosol hygroscopicity parameter derived from the light scattering enhancement factor measurements in the North China Plain, *Atmos. Chem. Phys.*, 14, 8105–8118, doi:10.5194/acp-14-8105-2014, 2014.
- Cheng, Y., Zheng, G., Wei, C., Mu, Q., Zheng, B., Wang, Z., Gao, M., Zhang, Q., He, K., Carmichael, G., Pöschl, U. and Su, H.: Reactive nitrogen chemistry in aerosol water as a source of sulfate during haze events in China, *Science Advances*, 2(12), e1601530–e1601530, doi:10.1126/sciadv.1601530, 2016b.
- Ding, A. J., Huang, X., Nie, W., Sun, J. N., Kerminen, V. M., Petäjä, T., Su, H., Cheng, Y. F., Yang, X. Q., Wang, M. H., Chi, X. G., Wang, J. P., Virkkula, A., Guo, W. D., Yuan, J., Wang, S. Y., Zhang, R. J., Wu, Y. F., Song, Y., Zhu, T., Zilitinkevich, S., Kulmala, M. and Fu, C. B.: Enhanced haze pollution by black carbon in megacities in China, *Geophysical Research Letters*, 43(6), 2873–2879, doi:10.1002/2016GL067745, 2016.

Eresmaa, N., Härkönen, J., Joffre, S. M., Schultz, D. M., Karppinen, A. and Kukkonen, J.: A Three-Step Method for Estimating the Mixing Height Using Ceilometer Data from the Helsinki Testbed, *Journal of Applied Meteorology and Climatology*, 51(12), 2172–2187, doi:10.1175/JAMC-D-12-058.1, 2012.

Fountoukis, C. and Nenes, A.: ISORROPIA II: a computationally efficient thermodynamic equilibrium model for

$K^+$ – $Ca^{2+}$ – $Mg^{2+}$ – $NH_4^+$ – $Na^+$ – $SO_4^{2-}$ – $NO_3$ , *Atmospheric Chemistry and Physics*, 7(17), 4639–4659, doi:10.5194/acp-7-4639-2007, 2007.

Fröhlich, R., Cubison, M. J., Slowik, J. G., Bukowiecki, N., Prévôt, A. S. H., Baltensperger, U., Schneider, J., Kimmel, J. R., Gonin, M., Rohner, U., Worsnop, D. R. and Jayne, J. T.: The ToF-ACSM: A portable aerosol chemical speciation monitor with TOFMS detection, *Atmospheric Measurement Techniques*, 6(11), 3225–3241, doi:10.5194/amt-6-3225-2013, 2013.

Gysel, M., Crosier, J., Topping, D. O., Whitehead, J. D., Bower, K. N., Cubison, M. J., Williams, P. I., Flynn, M. J., McFiggans, G. B. and Coe, H.: Closure study between chemical composition and hygroscopic growth of aerosol particles during TORCH2, *Atmospheric Chemistry and Physics*, 7(24), 6131–6144, doi:10.5194/acp-7-6131-2007, 2007.

Holzworth, G. C.: Mixing heights, wind speeds, and potential for urban air pollution throughout the contiguous united states, , 118, 1972.

Jimenez, J. L., Canagaratna, M. R., Donahue, N. M., Prevot, A. S. H., Zhang, Q., Kroll, J. H., DeCarlo, P. F., Allan, J. D., Coe, H., Ng, N. L., Aiken, A. C., Docherty, K. S., Ulbrich, I. M., Grieshop, A. P., Robinson, A. L., Duplissy, J., Smith, J. D., Wilson, K. R., Lanz, V. A., Hueglin, C., Sun, Y. L., Tian, J., Laaksonen, A., Raatikainen, T., Rautiainen, J., Vaattovaara, P., Ehn, M., Kulmala, M., Tomlinson, J. M., Collins, D. R., Cubison, M. J., Dunlea, E. J., Huffman, J. A., Onasch, T. B., Alfarra, M. R., Williams, P. I., Bower, K., Kondo, Y., Schneider, J., Drewnick, F., Borrmann, S., Weimer, S., Demerjian, K., Salcedo, D., Cottrell, L., Griffin, R., Takami, A., Miyoshi, T., Hatakeyama, S., Shimojo, A., Sun, J. Y., Zhang, Y. M., Dzepina, K., Kimmel, J. R., Sueper, D., Jayne, J. T., Herndon, S. C., Trimborn, A. M., Williams, L. R., Wood, E. C., Middlebrook, A. M., Kolb, C. E., Baltensperger, U. and Worsnop, D. R.: Evolution of organic

aerosols in the atmosphere, *Science*, 326(5959), 1525–1529, doi:10.1126/science.1180353, 2009.

Jokinen, T., Sipilä, M., Junninen, H., Ehn, M., Lönn, G., Hakala, J., Petäjä, T., Mauldin, R. L., Kulmala, M. and Worsnop, D. R.: Atmospheric sulphuric acid and neutral cluster measurements using CI-API-TOF, *Atmospheric Chemistry and Physics*, 12(9), 4117–4125, doi:10.5194/acp-12-4117-2012, 2012.

Lelieveld, J., Evans, J. S., Fnais, M., Giannadaki, D. and Pozzer, A.: The contribution of outdoor air pollution sources to premature mortality on a global scale, *Nature*, 525(7569), 367–371, doi:10.1038/nature15371, 2015.

Li, H., Zhang, Q., Zheng, B., Chen, C., Wu, N., Guo, H., Zhang, Y., Zheng, Y., Li, X. and He, K.: Nitrate-driven urban haze pollution during summertime over the North China Plain, *Atmospheric Chemistry and Physics*, 18(8), 5293–5306, doi:10.5194/acp-18-5293-2018, 2018a.

Li, J., Sun, J., Zhou, M., Cheng, Z., Li, Q., Cao, X. and Zhang, J.: Observational analyses of dramatic developments of a severe air pollution event in the Beijing area, *Atmospheric Chemistry and Physics*, 18(6), 3919–3935, doi:10.5194/acp-18-3919-2018, 2018b.

Lin, Z. J., Tao, J., Chai, F. H., Fan, S. J., Yue, J. H., Zhu, L. H., Ho, K. F. and Zhang, R. J.: Impact of relative humidity and particles number size distribution on aerosol light extinction in the urban area of Guangzhou, *Atmospheric Chemistry and Physics*, 13(3), 1115–1128, doi:10.5194/acp-13-1115-2013, 2013.

Liu, G., Xin, J., Wang, X., Si, R., Ma, Y., Wen, T., Zhao, L., Zhao, D., Wang, Y. and Gao, W.: Impact of the coal banning zone on visibility in the Beijing-Tianjin-Hebei region, *Science of the Total Environment*, 692, 402–410, doi:10.1016/j.scitotenv.2019.07.006, 2019a.

Liu, Q., Jia, X., Quan, J., Li, J., Li, X., Wu, Y., Chen, D., Wang, Z. and Liu, Y.: New positive feedback mechanism between boundary layer meteorology and secondary aerosol formation during severe haze events, *Scientific Reports*, 8(1), doi:10.1038/s41598-018-24366-3, 2018.

Liu, Y., Zhang, Y., Lian, C., Yan, C. and Feng, Z.: The promotion effect of nitrous acid on aerosol formation in wintertime Beijing : possible contribution of traffic-related emission, *Atmos. Chem. Phys. Discuss.*, 2020(February), 1–43, doi:10.5194/acp-2020-150, 2020.

Liu, Z., Hu, B., Ji, D., Cheng, M., Gao, W., Shi, S., Xie, Y., Yang, S., Gao, M., Fu, H., Chen, J. and

- Wang, Y.: Characteristics of fine particle explosive growth events in Beijing, China: Seasonal variation, chemical evolution pattern and formation mechanism, *Science of the Total Environment*, 687, 1073–1086, doi:10.1016/j.scitotenv.2019.06.068, 2019b.
- Münkel, C., Eresmaa, N., Räsänen, J. and Karppinen, A.: Retrieval of mixing height and dust concentration with lidar ceilometer, *Boundary-Layer Meteorology*, 124(1), 117–128, doi:10.1007/s10546-006-9103-3, 2007.
- Pan, X. L., Yan, P., Tang, J., Ma, J. Z., Wang, Z. F., Gbaguidi, A. and Sun, Y. L.: Observational study of influence of aerosol hygroscopic growth on scattering coefficient over rural area near Beijing mega-city, *Atmospheric Chemistry and Physics*, 9(19), 7519–7530, doi:10.5194/acp-9-7519-2009, 2009.
- Pan, Y., Tian, S., Liu, D., Fang, Y., Zhu, X., Zhang, Q., Zheng, B., Michalski, G. and Wang, Y.: Fossil Fuel Combustion-Related Emissions Dominate Atmospheric Ammonia Sources during Severe Haze Episodes: Evidence from  $^{15}\text{N}$ -Stable Isotope in Size-Resolved Aerosol Ammonium, *Environmental Science and Technology*, 50(15), 8049–8056, doi:10.1021/acs.est.6b00634, 2016.
- Petäjä, T., Järvi, L., Kerminen, V. M., Ding, A. J., Sun, J. N., Nie, W., Kujansuu, J., Virkkula, A., Yang, X., Fu, C. B., Zilitinkevich, S. and Kulmala, M.: Enhanced air pollution via aerosol-boundary layer feedback in China, *Scientific Reports*, 6, doi:10.1038/srep18998, 2016.
- Pieber, S. M., El Haddad, I., Slowik, J. G., Canagaratna, M. R., Jayne, J. T., Platt, S. M., Bozzetti, C., Daellenbach, K. R., Fröhlich, R., Vlachou, A., Klein, F., Dommen, J., Miljevic, B., Jiménez, J. L., Worsnop, D. R., Baltensperger, U. and Prévôt, A. S. H.: Inorganic Salt Interference on  $\text{CO}_2^+$  in Aerodyne AMS and ACSM Organic Aerosol Composition Studies, *Environmental Science and Technology*, 50(19), 10494–10503, doi:10.1021/acs.est.6b01035, 2016.
- Spracklen, D. V., Carslaw, K. S., Kulmala, M., Kerminen, V. M., Sihto, S. L., Riipinen, I., Merikanto, J., Mann, G. W., Chipperfield, M. P., Wiedensohler, A., Birmili, W. and Lihavainen, H.: Contribution of particle formation to global cloud condensation nuclei concentrations, *Geophysical Research Letters*, 35(6), doi:10.1029/2007GL033038, 2008.
- Stohl, A., Forster, C., Frank, A., Seibert, P. and Wotawa, G.: Technical note: The Lagrangian particle dispersion model FLEXPART version 6.2, *Atmospheric Chemistry and Physics*, 5(9),

2461–2474, doi:10.5194/acp-5-2461-2005, 2005.

Swietlicki, E., Hansson, H.-C., Hämeri, K., Svenningsson, B., Massling, A., Mcfiggans, G., McMurry, P. H., Petäjä, T., Tunved, P., Gysel, M., Topping, D., Weingartner, E., Baltensperger, U., Rissler, J., Wiedensohler, A. and Kulmala, M.: Hygroscopic properties of submicrometer atmospheric aerosol particles measured with H-TDMA instruments in various environments—a review, *Tellus B: Chemical and Physical Meteorology*, 60(3), 432–469, doi:10.1111/j.1600-0889.2008.00350.x, 2008.

Tang, G., Zhang, J., Zhu, X., Song, T., Munkel, C., Hu, B., Schäfer, K., Liu, Z., Zhang, J., Wang, L., Xin, J., Suppan, P. and Wang, Y.: Mixing layer height and its implications for air pollution over Beijing, China, *Atmos. Chem. Phys*, 16, 2459–2475, doi:10.5194/acp-16-2459-2016, 2016.

Titos, G., Cazorla, A., Zieger, P., Andrews, E., Lyamani, H., Granados-Muñoz, M. J., Olmo, F. J. and Alados-Arboledas, L.: Effect of hygroscopic growth on the aerosol light-scattering coefficient: A review of measurements, techniques and error sources, *Atmospheric Environment*, 141, 494–507, doi:10.1016/j.atmosenv.2016.07.021, 2016.

Vanhanen, J., Mikkilä, J., Lehtipalo, K., Sipilä, M., Manninen, H. E., Siivola, E., Petäjä, T. and Kulmala, M.: Particle size magnifier for nano-CN detection, *Aerosol Science and Technology*, 45(4), 533–542, doi:10.1080/02786826.2010.547889, 2011.

Wang, G., Zhang, R., Gomez, M. E., Yang, L., Zamora, M. L., Hu, M., Lin, Y., Peng, J., Guo, S., Meng, J., Li, J., Cheng, C., Hu, T., Ren, Y., Wang, Y., Gao, J., Cao, J., An, Z., Zhou, W., Li, G., Wang, J., Tian, P., Marrero-Ortiz, W., Secret, J., Du, Z., Zheng, J., Shang, D., Zeng, L., Shao, M., Wang, W., Huang, Y., Wang, Y., Zhu, Y., Li, Y., Hu, J., Pan, B., Cai, L., Cheng, Y., Ji, Y., Zhang, F., Rosenfeld, D., Liss, P. S., Duce, R. A., Kolb, C. E. and Molina, M. J.: Persistent sulfate formation from London Fog to Chinese haze, *Proceedings of the National Academy of Sciences of the United States of America*, 113(48), 13630–13635, doi:10.1073/pnas.1616540113, 2016.

Wang, H., Peng, Y., Zhang, X., Liu, H., Zhang, M., Che, H. and Cheng, Y.: Contributions to the explosive growth of PM<sub>2.5</sub> mass due to aerosol – radiation feedback and decrease in turbulent diffusion during a red alert heavy haze in Beijing – Tianjin – Hebei, China, , 17717–17733, 2018a.

Wang, J., Wang, S., Jiang, J., Ding, A., Zheng, M., Zhao, B., Wong, D. C., Zhou, W., Zheng, G.,

Wang, L., Pleim, J. E. and Hao, J.: Impact of aerosol-meteorology interactions on fine particle pollution during China's severe haze episode in January 2013, *Environmental Research Letters*, 9(9), doi:10.1088/1748-9326/9/9/094002, 2014a.

Wang, M., Kong, W., Marten, R., He, X.-C., Chen, D., Pfeifer, J., Heitto, A., Kontkanen, J., Dada, L., Kürten, A., Yli-Juuti, T., Manninen, H. E., Amanatidis, S., Amorim, A., Baalbaki, R., Baccarini, A., Bell, D. M., Bertozzi, B., Bräkling, S., Brilke, S., Murillo, L. C., Chiu, R., Chu, B., De Menezes, L.-P., Duplissy, J., Finkenzeller, H., Carracedo, L. G., Granzin, M., Guida, R., Hansel, A., Hofbauer, V., Krechmer, J., Lehtipalo, K., Lamkaddam, H., Lampimäki, M., Lee, C. P., Makhmutov, V., Marie, G., Mathot, S., Mauldin, R. L., Mentler, B., Müller, T., Onnela, A., Partoll, E., Petäjä, T., Philippov, M., Pospisilova, V., Ranjithkumar, A., Rissanen, M., Rörup, B., Scholz, W., Shen, J., Simon, M., Sipilä, M., Steiner, G., Stolzenburg, D., Tham, Y. J., Tomé, A., Wagner, A. C., Wang, D. S., Wang, Y., Weber, S. K., Winkler, P. M., Wlasits, P. J., Wu, Y., Xiao, M., Ye, Q., Zauner-Wieczorek, M., Zhou, X., Volkamer, R., Riipinen, I., Dommen, J., Curtius, J., Baltensperger, U., Kulmala, M., Worsnop, D. R., Kirkby, J., Seinfeld, J. H., El-Haddad, I., Flagan, R. C. and Donahue, N. M.: Rapid growth of new atmospheric particles by nitric acid and ammonia condensation, *Nature*, 581(7807), 184–189, doi:10.1038/s41586-020-2270-4, 2020d.

Wang, X., Wang, T., Yan, C., Tham, Y. J., Xue, L., Xu, Z. and Zha, Q.: Large daytime signals of N<sub>2</sub>O<sub>5</sub> and NO<sub>3</sub> inferred at 62 amu in a TD-CIMS: Chemical interference or a real atmospheric phenomenon, *Atmospheric Measurement Techniques*, 7(1), 1–12, doi:10.5194/amt-7-1-2014, 2014b.

Wang, Y., Riva, M., Xie, H. and Heikkinen, L.: Formation of highly oxygenated organic molecules from chlorine atom initiated oxidation of alpha-pinene, *Atmospheric Chemistry and Physics*, 2020, 1–31, doi:10.5194/acp-2019-807, 2020.

Wang, Y., Wang, Y., Wang, L., Petäjä, T., Zha, Q., Gong, C., Li, S., Pan, Y., Hu, B., Xin, J. and Kulmala, M.: Increased inorganic aerosol fraction contributes to air pollution and haze in China, *Atmos. Chem. Phys.*, 19, 5881–5888, doi:10.5194/acp-19-5881-2019, 2019b.

Wang, Y., Gao, W., Wang, S., Song, T., Gong, Z., Ji, D., Wang, L., Liu, Z., Tang, G., Huo, Y., Tian, S., Li, J., Li, M., Yang, Y., Chu, B., Petäjä, T., Kerminen, V.-M., He, H., Hao, J., Kulmala,

- M., Wang, Y. and Zhang, Y.: Contrasting trends of PM<sub>2.5</sub> and surface ozone concentrations in China from 2013 to 2017, *National Science Review*, doi:10.1093/nsr/nwaa032, 2020b.
- Wang, Y., Chen, Y., Wu, Z., Shang, D., Bian, Y., Du, Z. and Schmitt, S. H.: Mutual promotion between aerosol particle liquid water and particulate nitrate enhancement leads to severe nitrate-dominated particulate matter pollution and low visibility, *Atmos. Chem. Phys.*, (September 2020), 2161–2175, 2020c.
- Wang, Y., Yu, M., Wang, Y., Tang, G., Song, T., Zhou, P., Liu, Z., Hu, B., Ji, D., Wang, L., Zhu, X., Yan, C., Ehn, M., Gao, W., Pan, Y., Xin, J., Sun, Y., Kerminen, V.-M., Kulmala, M. and Petäjä, T.: Rapid formation of intense haze episodes via aerosol–boundary layer feedback in Beijing, *Atmos. Chem. Phys.*, 20(1), 45–53, doi:10.5194/acp-20-45-2020, 2020d.
- Wang, Y. H., Hu, B., Ji, D. S., Liu, Z. R., Tang, G. Q., Xin, J. Y., Zhang, H. X., Song, T., Wang, L. L., Gao, W. K., Wang, X. K. and Wang, Y. S.: Ozone weekend effects in the Beijing-Tianjin-Hebei metropolitan area, China, *Atmos. Chem. Phys.*, 14, 2419–2429, doi:10.5194/acp-14-2419-2014, 2014c.
- Wang, Y. H., Liu, Z. R., Zhang, J. K., Hu, B., Ji, D. S., Yu, Y. C. and Wang, Y. S.: Aerosol physicochemical properties and implications for visibility during an intense haze episode during winter in Beijing, *Atmospheric Chemistry and Physics*, 15(6), 3205–3215, doi:10.5194/acp-15-3205-2015, 2015.
- Wu, Z., Wang, Y., Tan, T., Zhu, Y., Li, M., Shang, D., Wang, H., Lu, K., Guo, S., Zeng, L. and Zhang, Y.: Aerosol Liquid Water Driven by Anthropogenic Inorganic Salts: Implying Its Key Role in Haze Formation over the North China Plain, *Environmental Science and Technology Letters*, 5(3), 160–166, doi:10.1021/acs.estlett.8b00021, 2018.
- Xie, Y., Ding, A., Nie, W., Mao, H., Qi, X., Huang, X., Xu, Z., Kerminen, V. M., Petäjä, T., Chi, X., Virkkula, A., Boy, M., Xue, L., Guo, J., Sun, J., Yang, X., Kulmala, M. and Fu, C.: Enhanced sulfate formation by nitrogen dioxide: Implications from in-situ observations at the SORPES station, *Journal of Geophysical Research*, 120(24), 12,679–12,694, doi:10.1002/2015JD023607, 2015.
- Xue, J., Yuan, Z., Griffith, S. M., Yu, X., Lau, A. K. H. and Yu, J. Z.: Sulfate Formation Enhanced



by a Cocktail of High NO<sub>x</sub>, SO<sub>2</sub>, Particulate Matter, and Droplet pH during Haze-Fog Events in Megacities in China: An Observation-Based Modeling Investigation, *Environmental Science and Technology*, 50(14), 7325–7334, doi:10.1021/acs.est.6b00768, 2016.

Xue, J., Yu, X., Yuan, Z., Griffith, S. M., Lau, A. K. H., Seinfeld, J. H. and Yu, J. Z.: Efficient control of atmospheric sulfate production based on three formation regimes, *Nature Geoscience*, 12(12), 1–6, doi:10.1038/s41561-019-0485-5, 2019.

Zheng, B., Tong, D., Li, M., Liu, F., Hong, C., Geng, G., Li, H., Li, X., Peng, L., Qi, J., Yan, L., Zhang, Y., Zhao, H., Zheng, Y., He, K. and Zhang, Q.: Trends in China's anthropogenic emissions since 2010 as the consequence of clean air actions, *Atmospheric Chemistry and Physics Discussions*, 1–27, doi:10.5194/acp-2018-374, 2018.

Zhong, J., Zhang, X., Dong, Y., Wang, Y., Liu, C., Wang, J., Zhang, Y. and Che, H.: Feedback effects of boundary-layer meteorological factors on cumulative explosive growth of PM<sub>2.5</sub> during winter heavy pollution episodes in Beijing from 2013 to 2016, *Atmospheric Chemistry and Physics*, 18(1), 247–258, doi:10.5194/acp-18-247-2018, 2018.

Zhou, Y., Dada, L., Liu, Y., Fu, Y., Kangasluoma, J., Chan, T., Yan, C., Chu, B., Daellenbach, K. R., Bianchi, F., Kokkonen, T. V., Liu, Y., Kujansuu, J., Kerminen, V.-M., Petäjä, T., Wang, L., Jiang, J. and Kulmala, M.: Variation of size-segregated particle number concentrations in wintertime Beijing, *Atmospheric Chemistry and Physics*, 20(2), 1201–1216, doi:10.5194/acp-20-1201-2020, 2020.

416

417

418

419

420

421

422

423

424

Figure caption

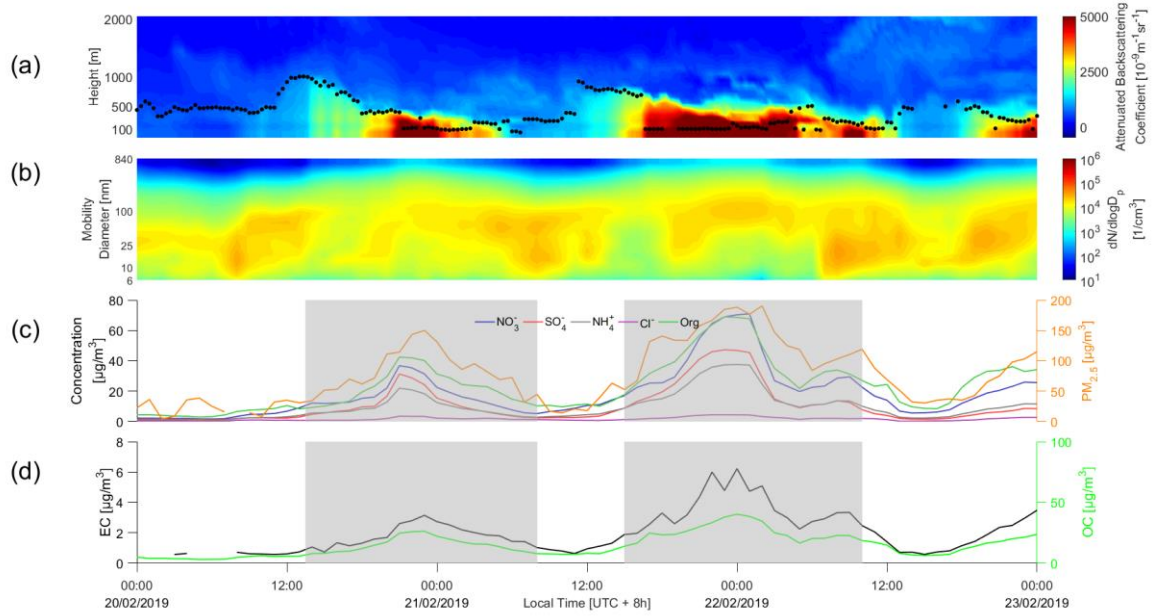


Figure 1. Time series of (a) attenuated backscattering coefficient and mixing layer height (b) particle number concentration distribution (PNSD), (c) chemical composition and  $\text{PM}_{2.5}$  mass concentrations and (d) elemental carbon (EC) and organic carbon (OC). The haze periods are marked by the shaded areas.

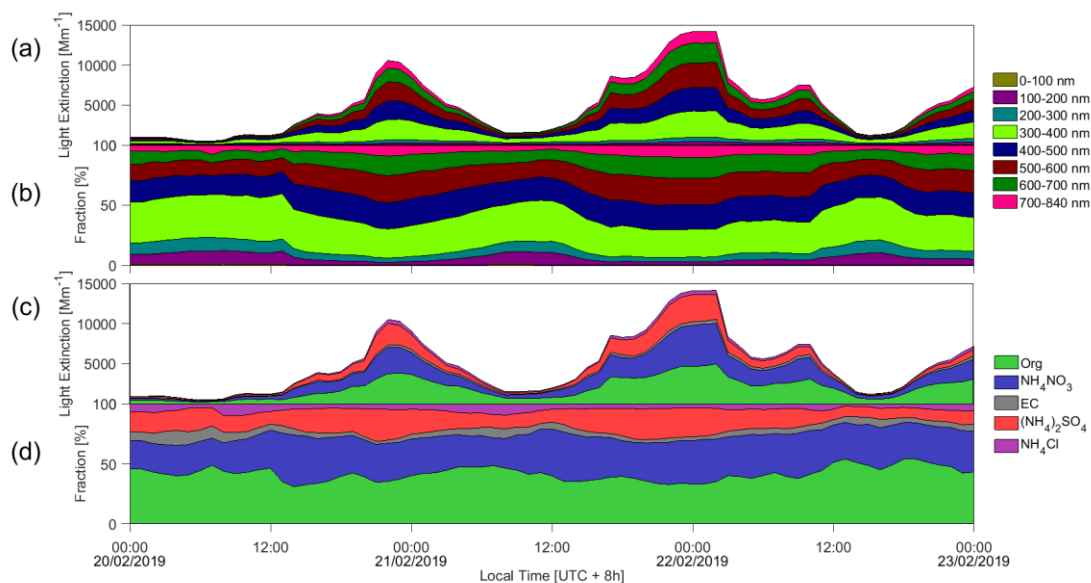


Figure 2. Time series of (a, b) variation of light extinction from different size aerosol and fractions, and (c, d) variation of light extinction from different aerosol species and fractions. The legends in the left side of figures are particle diameter and the right side are chemical compositions, respectively.

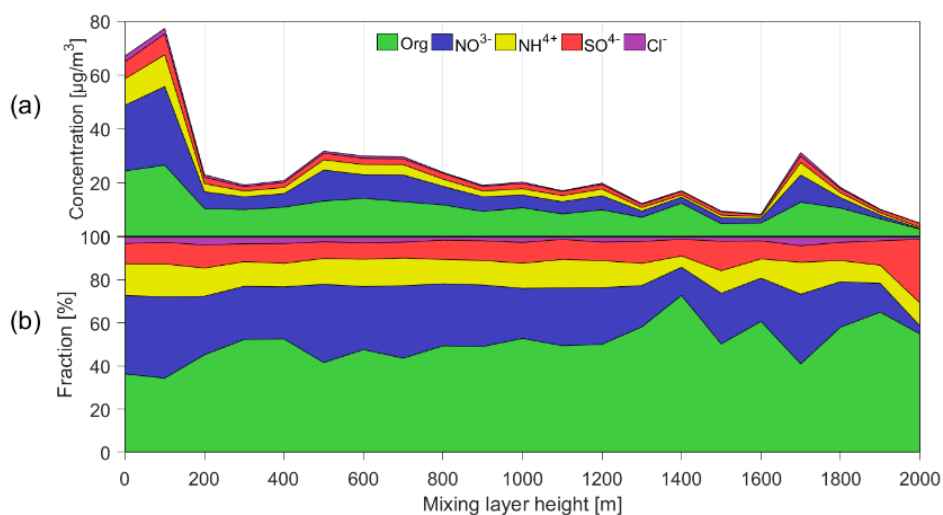


Figure 3. Statistical relationship between MLH and concentration (a) and fraction (b) of chemical composition species. Only daytime conditions determined by ceilometer from non-rainy periods (RH<95%) during the observation (~ 6 months) are considered.

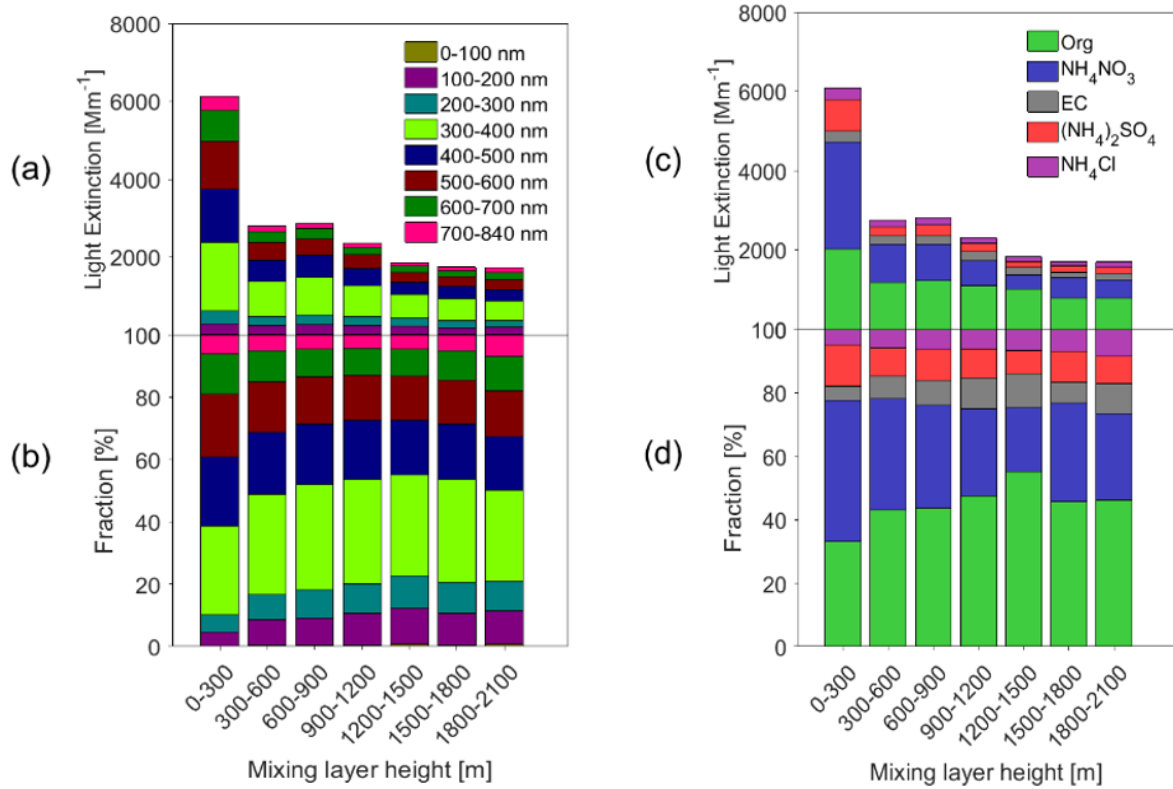
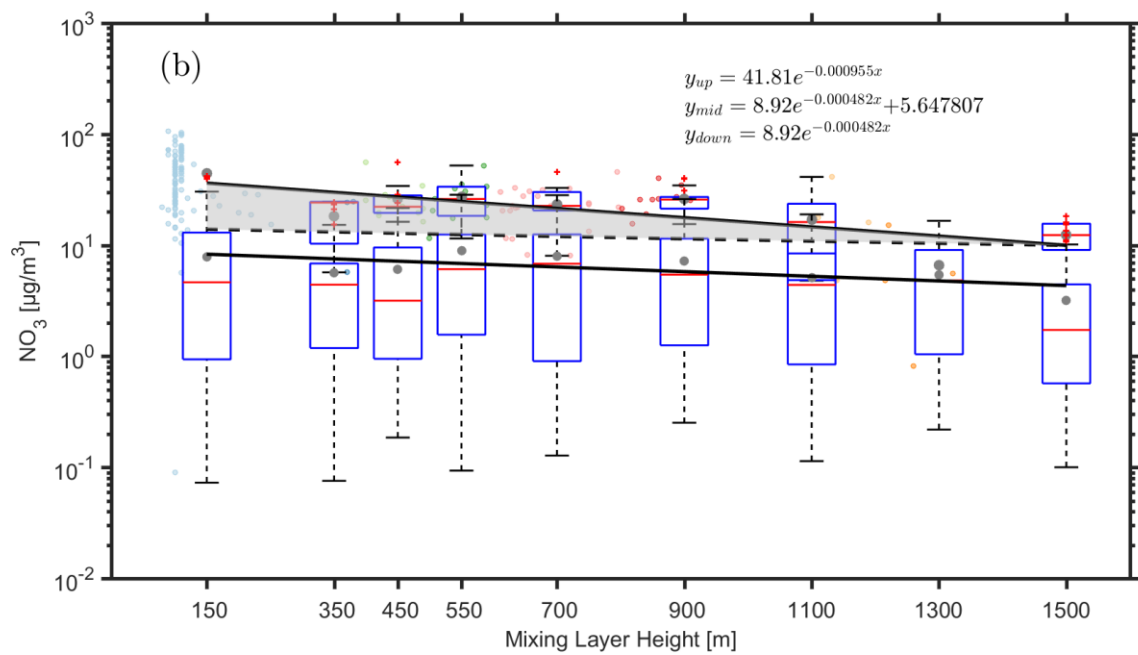
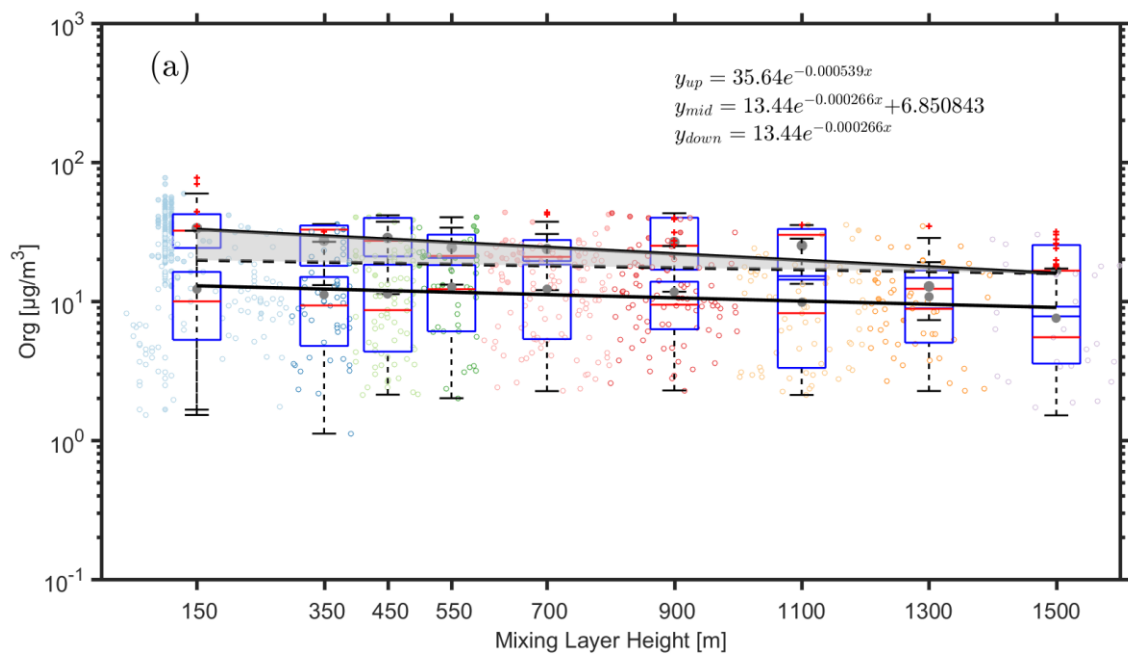
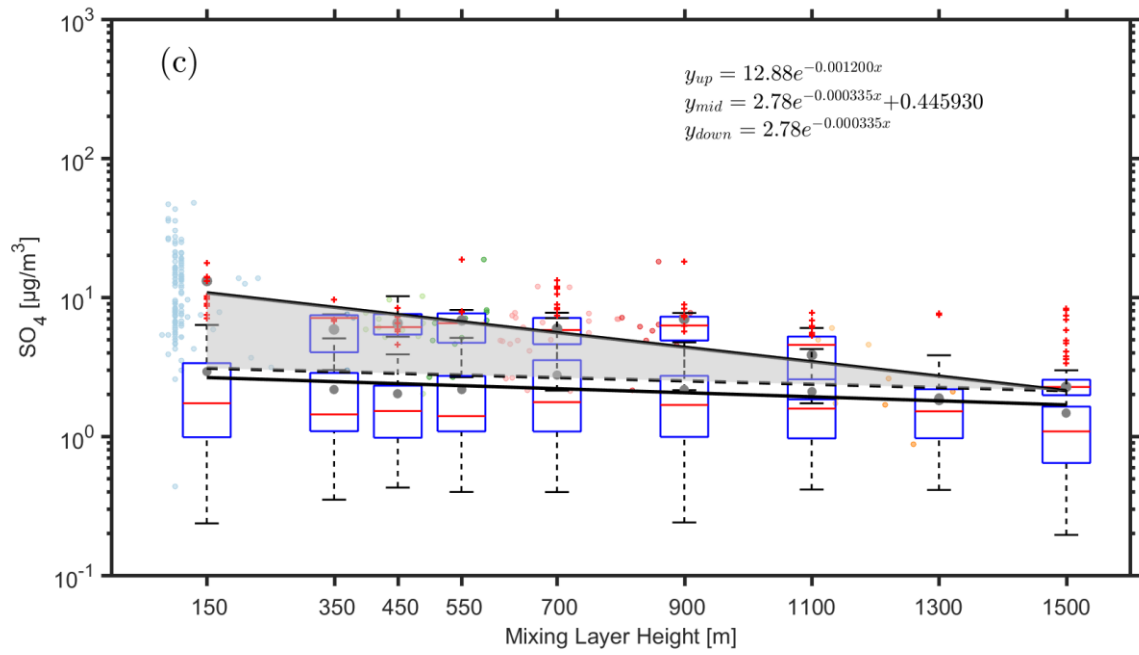


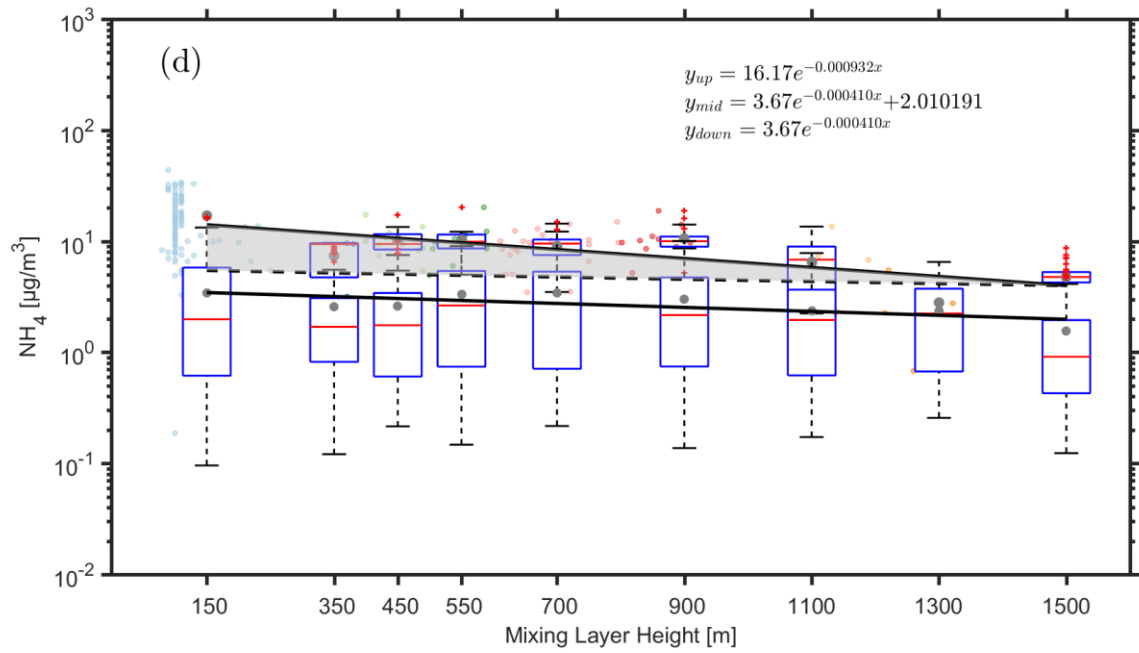
Figure 4. Statistical relationship between MLH and light extinction of different aerosol species. Only daytime conditions determined by the ceilometer from non-rainy periods ( $\text{RH} < 95\%$ ) are considered.

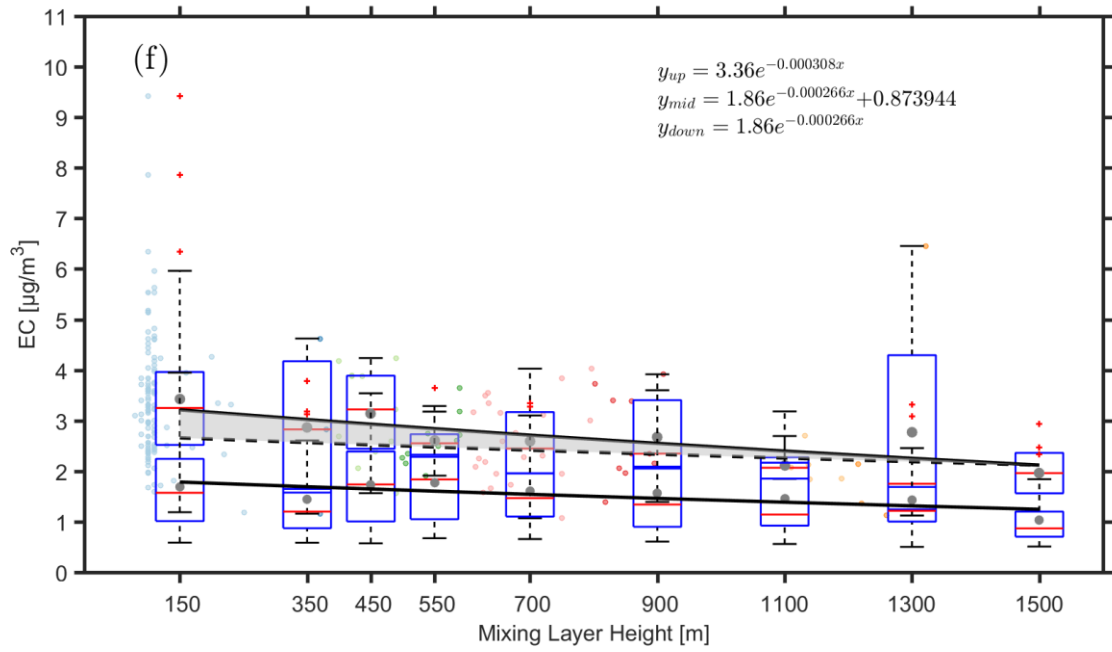
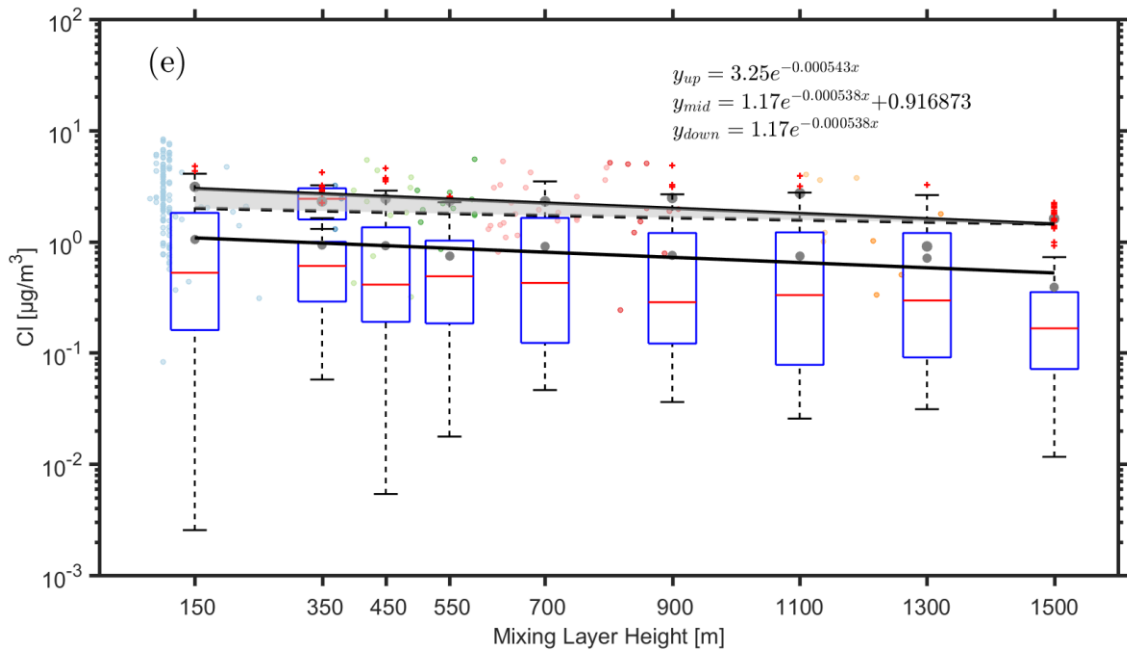


495

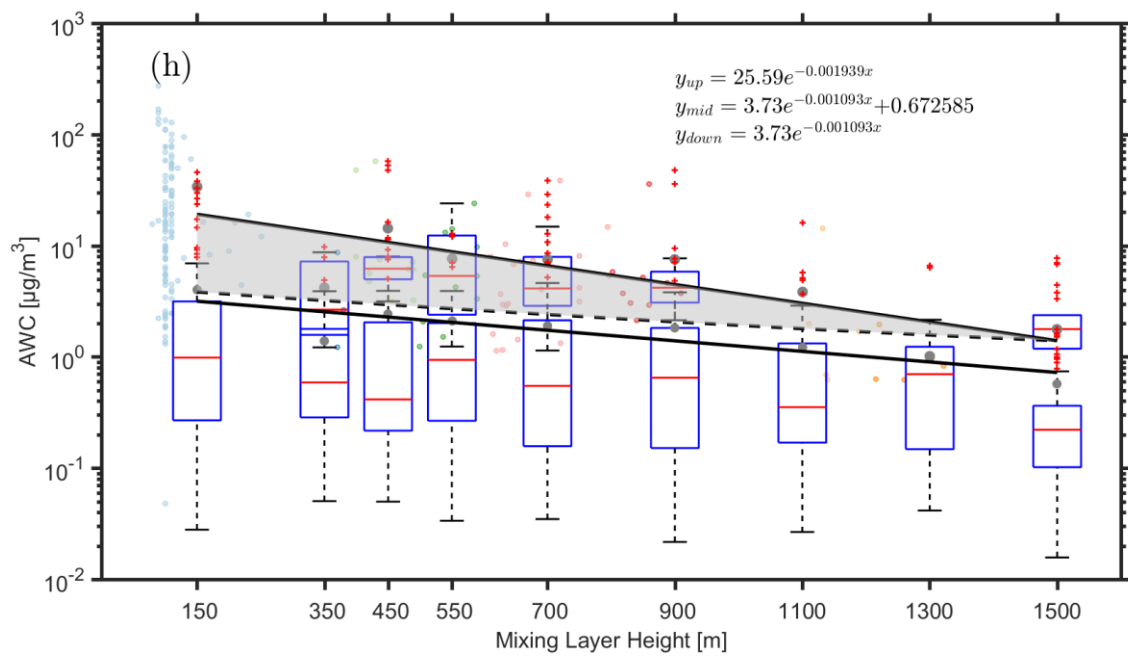
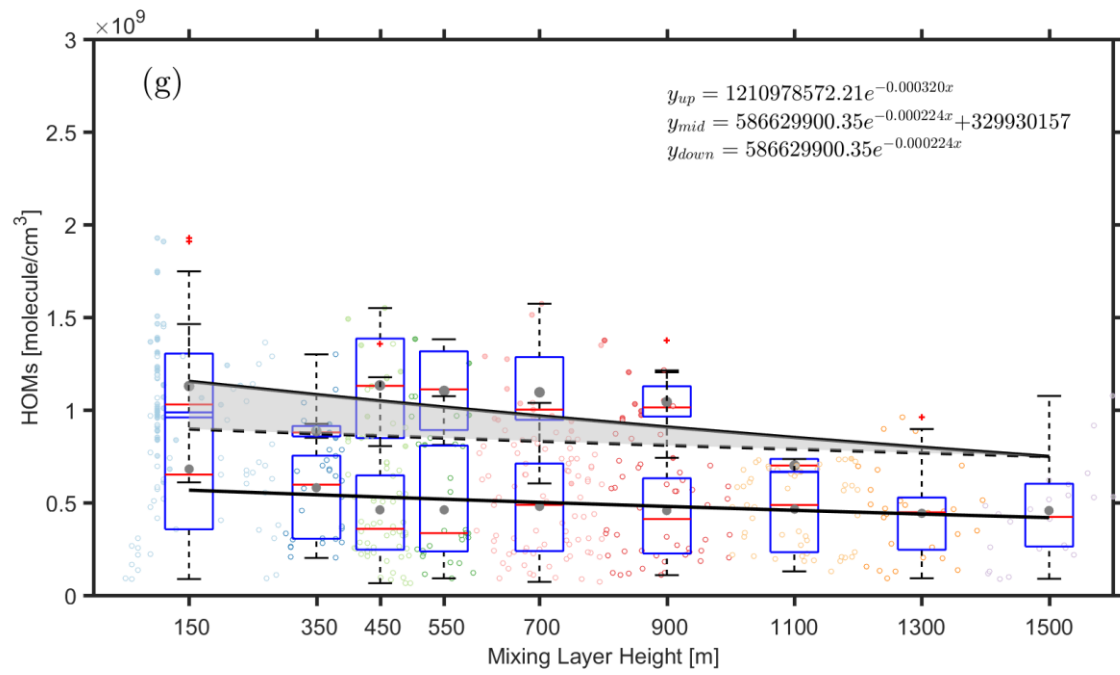


496









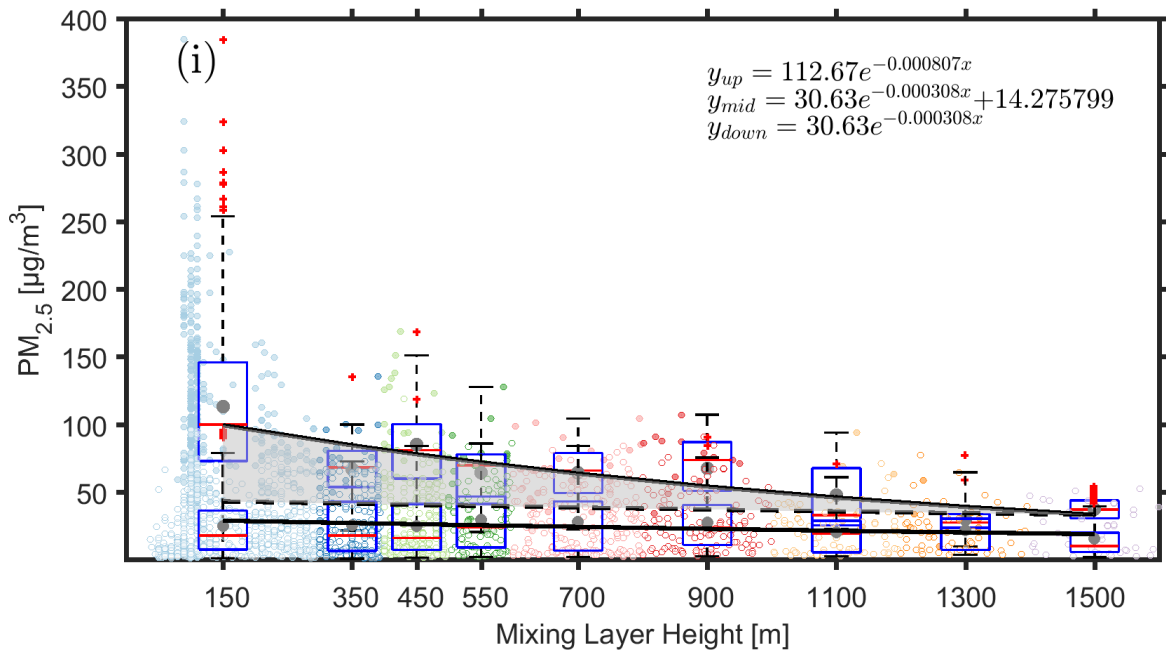
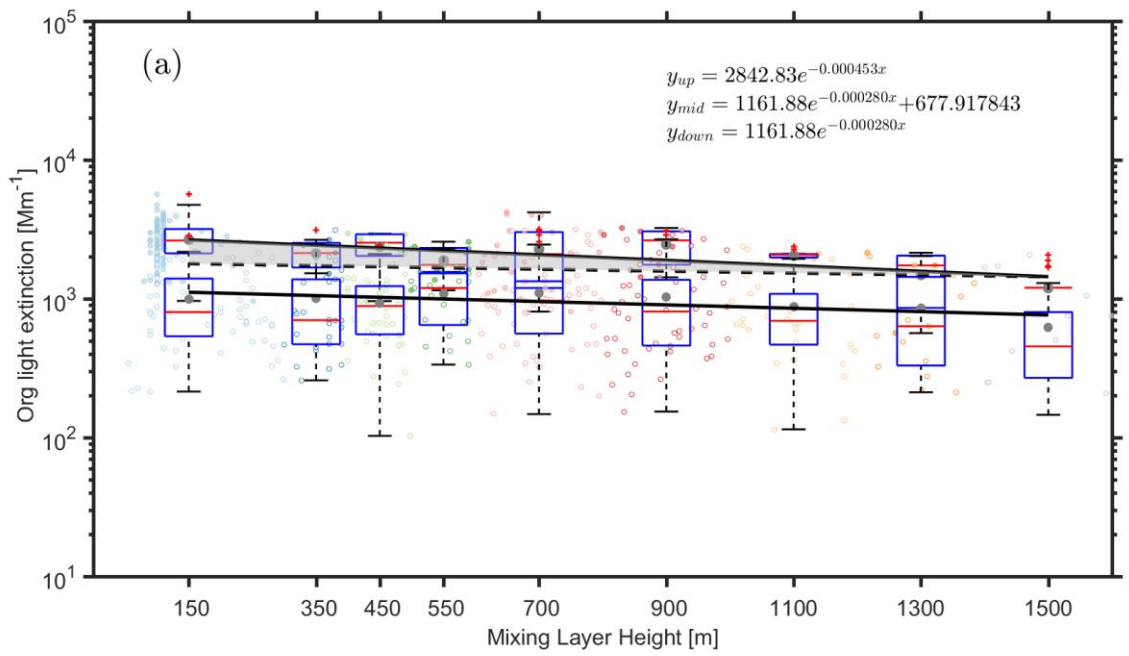
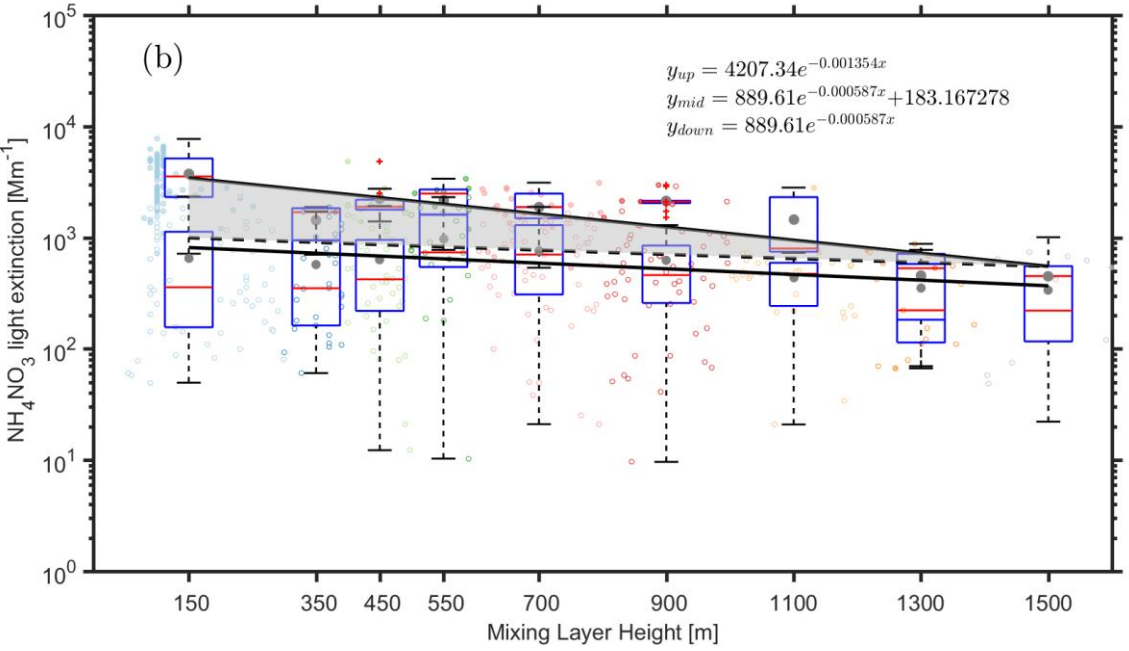


Figure 5. Observed dependency of (organics (a), nitrate (b), ammonium (c), sulfate (d), chlorine (e), element carbon (f), HOMs (g), AWC (h) and PM<sub>2.5</sub>(i) on the MLH during polluted and less-polluted conditions. The data related to the upper fitting line represents PM<sub>2.5</sub> concentrations larger than 75 µg m<sup>-3</sup>, while the data related to the lower fitting line represents PM<sub>2.5</sub> concentrations lower than 75 µg m<sup>-3</sup>. Only daytime conditions determined by the ceilometer from non-rainy periods (RH<95%) were considered. The solid cycles and hollow cycles denotes concentrations that are more than 75 µg m<sup>-3</sup> and less than 75 µg m<sup>-3</sup>, respectively. The dark grey points and red lines in the boxes represent mean and median values, respectively. The shaded area between the upper solid and dotted lines corresponds to an increased amount of the specific compounds with decreased MLH, assuming that the compound has the same variation pattern under highly- polluted conditions as in less polluted time.

523  
524  
525

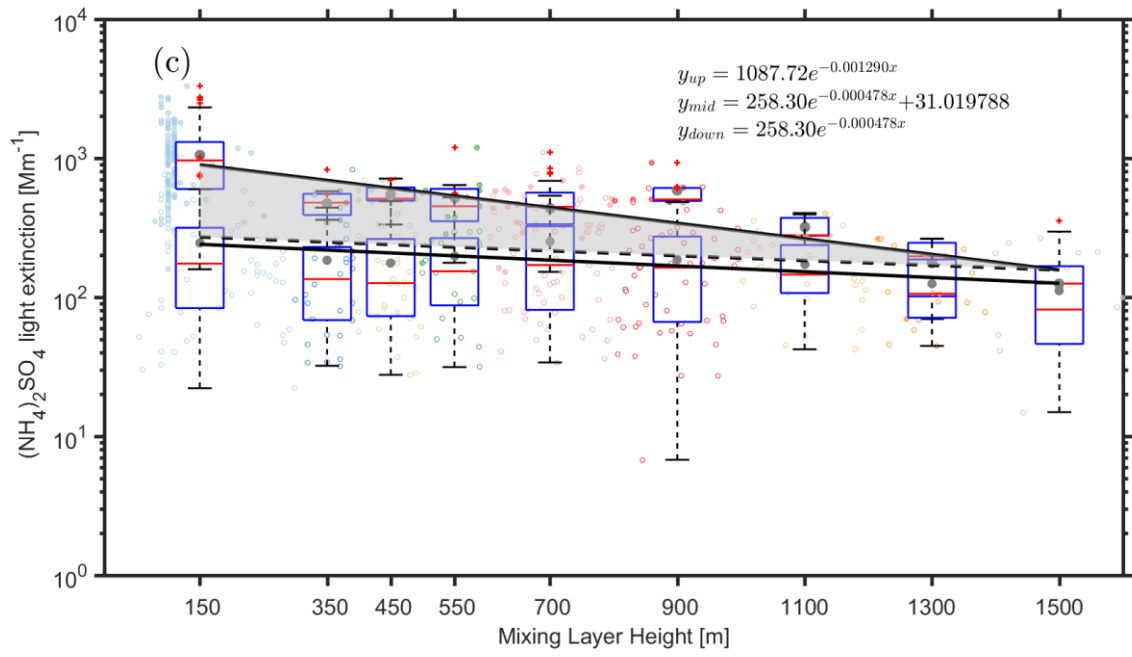


526

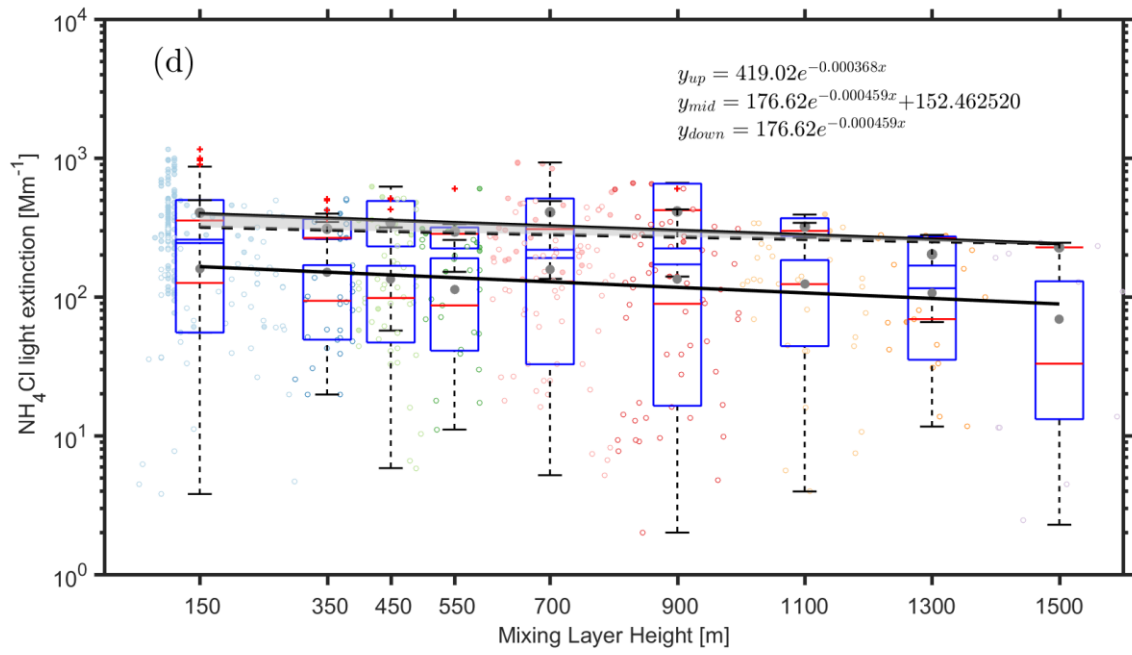


527

528



529



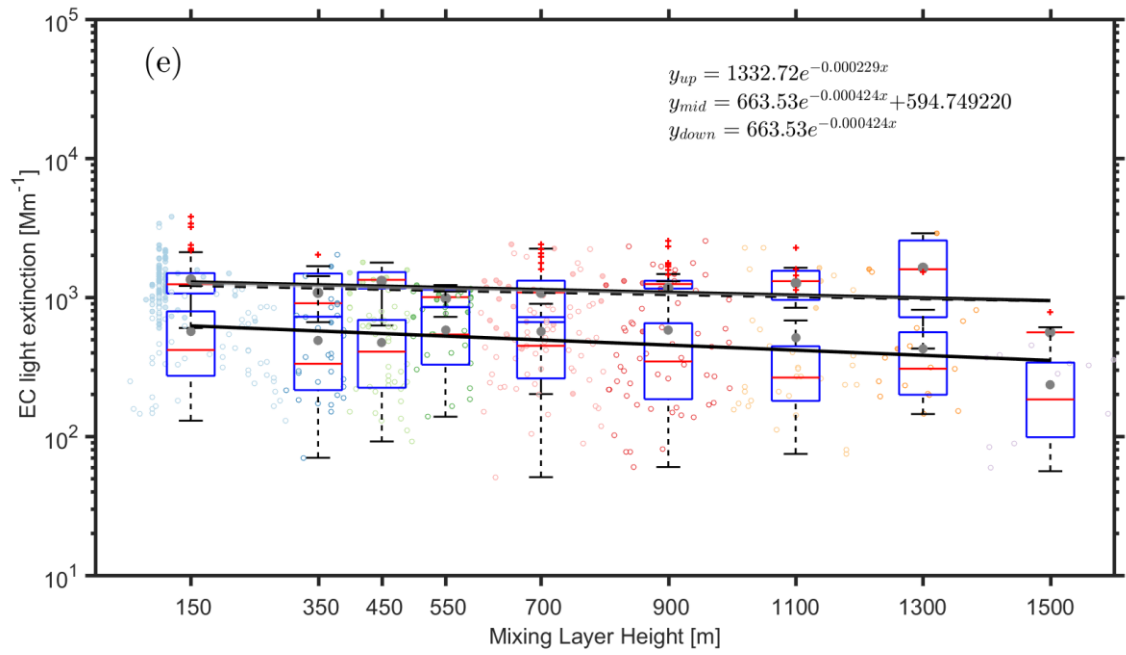


Figure 6. Observed dependency of the aerosol light extinction due to  $\text{NH}_4\text{NO}_3$  (a)  $(\text{NH}_4)_2\text{SO}_4$  (b),  $\text{NH}_4\text{Cl}$  (c) Org (d) and EC (e) on the MLH during polluted and non-polluted conditions. The data related to the upper fitting line represents  $\text{PM}_{2.5}$  concentrations larger than  $75 \mu\text{g m}^{-3}$ , while the data related to the lower fitting line represents  $\text{PM}_{2.5}$  concentrations less than  $75 \mu\text{g m}^{-3}$ . Only daytime conditions determined by ceilometer from non-rainy periods ( $\text{RH} < 95\%$ ) are considered. The dark grey points and red lines in the boxes represent mean and median values, respectively. The shaded area between the upper solid and dashed line corresponds to an increased amount of  $\text{PM}_{2.5}$  with a decreased MLH, assuming that  $\text{PM}_{2.5}$  has the same variation pattern under highly- polluted conditions as in less polluted time

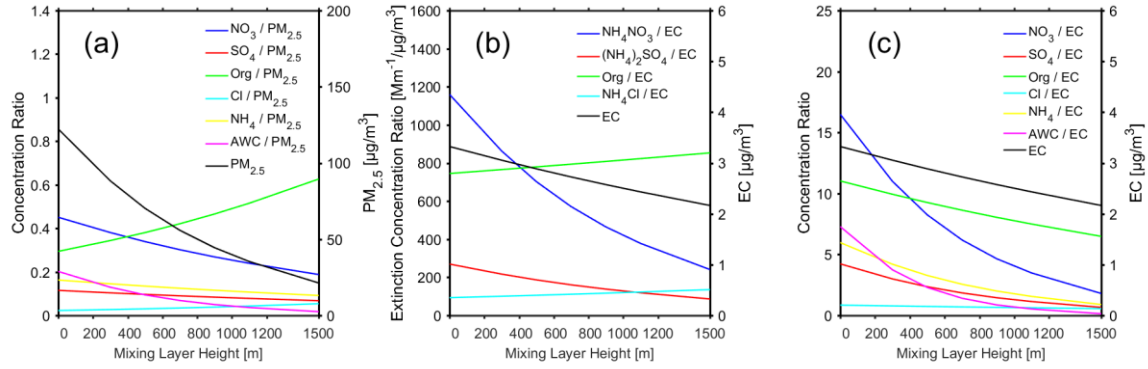


Figure 7. (a) the ratio of the mass concentration of different chemical components (nitrate, sulfate, organics, chlorine, ammonium) and AWC to the mass concentration of  $NR\_PM_{2.5}$  as a function of MLH. (b) the ratio of dry aerosol light extinction by different chemical components ( $NH_4NO_3$ ,  $(NH_4)_2SO_4$ , Org,  $NH_4Cl$ ) to the mass concentration EC as a function of MLH (c) the ratio of the mass concentration of different chemical components (nitrate, sulfate, organics, chlorine, ammonium) and AWC to the mass concentration of EC as a function of MLH. All the data corresponds to polluted conditions ( $\text{fine PM} > 75 \mu g m^{-3}$ ), and only daytime conditions determined by the ceilometer from non-rainy periods ( $RH < 95\%$ ) were considered.

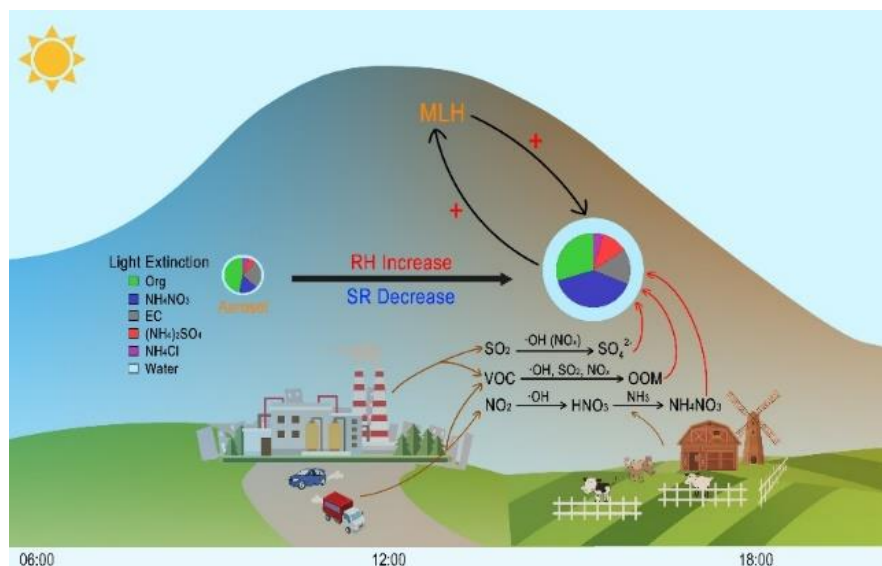


Figure 8. A schematic picture illustrating the process of rapid aerosol mass growth and enhanced light extinction in Beijing. The plus symbols represent the strengthening of a specific process. At the presence of aerosols during afternoon time in Beijing, the intensity of solar radiation reaching the surface will be decreased and relative humidity will be increased. As a result, the development of boundary layer will be suppressed, and the concentrations of aerosol precursors (e.g.,  $\text{SO}_2$ ,  $\text{NO}_2$ ,  $\text{VOC}$ ) will be increased. In turn, the secondary production of these sulfate, nitrate and oxygenated organic compounds will be enhanced due to increased concentrations and partitioning of these compounds into the aerosol phase. The increased formation of secondary aerosol mass will reduce solar radiation further and the haze formation increased, as shown in pie charts that the light extinction fraction of aerosol changed from organic to nitrate. Noting that during intensive haze periods, nitrate and its contribution to light extinction contribution increased dramatically.